applied sciences

MDPI

Review

Bond Characterization in Cementitious Material Binders Using Fourier-Transform Infrared Spectroscopy

Moruf Olalekan Yusuf

Department of Civil Engineering, College of Engineering, University of Hafr Al Batin, P.O. Box 1803, Hafr Al Batin 39524, Saudi Arabia; moruf@uhb.edu.sa

Abstract: Fourier-transform infrared (FTIR) spectroscopy is a fast and simple technique for functional group identification. This work provides a review and insight into the application and interpretation of FTIR spectroscopy for cementitious binders that comprise ordinary Portland cement, alkaline-activated binders, geopolymers, and material characterization for civil engineering material applications. This technique can be used to identify different compounds and a moiety of bond vibrations in inorganic molecules such as Si-O, -OH, H-O-H (water), C-O (carbonate or carbonation), aluminosilicate (Si-O-T, where T is Al or Si), and S-O (sulfate or gypsum) found in hydrated cement, alkaline binders, and geopolymers. The prominent bands include those representing carbonation (CO_3^{2-} 1390–1475 cm^{-1}), calcium carbonate (871, 1792–2516 cm^{-1}), hydroxylation and water molecules (1607, 3400–3650 cm^{-1}), strength skeletal framework compositions or Al-Si substitutions, silicate organization (C-A-S-H, N-A-S-H, or C-S-H (950–1055 cm^{-1}), and sulfate (600–680, 1080–1100 cm^{-1}). Some of the factors that could affect the spectra bands include elemental displacement due to changes in molar mass, activated temperature, pH, activator concentration, w/b ratio, Ca/Si ratio, Si/Al ratio, and the silica modulus (SiO_2/Na_2O) of the activators used in the binder synthesis. The method could be used for destructive and non-destructive testing on paste sample by using transmission and attenuated total reflectance methods, respectively.

Keywords: Fourier-transform infrared spectroscopy; geopolymers; alkaline-activated binder; material characterization; aluminosilicate materials

check for updates

Citation: Yusuf, M.O. Bond Characterization in Cementitious Material Binders Using Fourier-Transform Infrared Spectroscopy. *Appl. Sci.* **2023**, *13*, 3353. https://doi.org/10.3390/app13053353

Academic Editor: Eduardo Garzon

Received: 23 January 2023
Revised: 27 February 2023
Accepted: 1 March 2023
Published: 6 March 2023

Copyright: © 2023 by the author. Licensee MDPI, Basel, Switzerland. This article is an open access article distributed under the terms and conditions of the Creative Commons Attribution (CC BY) license (https://creativecommons.org/licenses/by/4.0/).

1. Introduction

The Fourier-transform infrared (FTIR) spectroscopy method is a method of bond characterization that could be used quantitatively and qualitatively with X-ray fluorescence (XRF), X-ray diffraction (XRD), scanning electron microscopy, and electron energy dispersive spectroscopy (SEM/EDS) to study the chemical composition, compound composition, microstructural morphology, and their elemental compositions in CB applications, respectively. Supplementary cementitious materials (SCMs) can be used in OPC to enhance secondary hydration. These SCMs can either be pozzolanic materials or hydraulic materials, such as ground granulated blast furnace slag (GGBFS) or pozzolanic materials, which comprise alumina and/or silica in significant quantities. Pozzolanic materials can also include fly ash (Class F), silica fume, metakaolin, palm oil fuel ash, glass waste, and rice husk ash [1,2]. Utilizing these materials in mortar and concrete productions reduces the carbon footprint and enhances cost-efficient materials for sustainable environments. These materials can be used as precursors for the synthesis of geopolymer (GP), alkaline-activated slag, or alkaline-activated binders (AABs). These precursors can also be named alkaline-activated materials (AAMs) [3,4]. Understanding the bond characterization of the binder through the application of the FTIR technique is quite helpful for the technical analysis of the binder with a view to controlling the strength and durability of the products [5–7]. Even though there have been a lot of reviews on the use of FTIR in different areas of applications, there has not been a full review in the literature on its application

and interpretation of the bond characterization in cementitious binders—ordinary Portland cement (OPC), alkaline-activated slag or binders (AAB/AAS), and geopolymers (GPs).

1.1. A Brief Background on the Use of FTIR in Material Characterization

Infrared (IR) light belongs to the spectrum whose frequency range lies between 4–140,000 cm^{-1}. It is bounded by microwaves and visible light. Generally, different parts of the electromagnetic spectrum are characterized by radiation velocity as well as the frequency which is inversely related to the wavelength [8]. There have been several applications of FTIR in different fields, such as the study of healthy and pathological blood samples and deducing molecular bond differences.

Furthermore, spectrometry has been used to study healthy and pathological blood samples in order to deduce molecular bond differences [9], organic chemistry [10], biomedical applications [11], and building diagnostics [12] in order to conserve energy and achieve a sustainable environment. In recent times, this technique is used for nano-particle detection, as reported by Hermann et al. [13], through its ability to identify bonds existing within the main compositions such as S-O bonds in gypsum, C-O in carbonates, hydroxyl (H-OH) groups, and aluminosilicates (Si-O-T; T is Si or Al) [14]. The purpose of FTIR is to provide additional information on X-ray diffraction (XRD) by relating bond characteristics to mineral characteristics. It remains a versatile tool for bond characterization of aluminosilicate and hydroxyl-based compounds. It could also be used to differentiate between amorphous and crystalline products with linear or cross-link chain products [12,15].

1.2. Mechanism of Fourier Infrared Spectroscopy

The mechanism of FTIR spectroscopy involves passing IR or signals of lumped frequencies from a polychromatic light source, such as a globar, an incandescent lamp, a nichrome wire, or a Nernst glower, to obtain mid-range IR radiation [16], whereas tungsten–halogen and mercury lamps can produce near and far IR, respectively [17]. The emitted radiation then travels via a collimator and Michelson interferometer (Figure 1), which consists of fixed mirrors, moveable mirrors, beam splitters, and helium–neon (He-Ne) laser beams. The beam splitter could be built of germanium coated with potassium bromide (KBr) and is used to split radiation into fixed and moveable mirrors prior to reflection and indentation on the sample [8]. Connecting the adjustable mirror to the He-Ne laser beam enables precise monitoring of its position, which has a direct correlation with optical path difference (OPD) and radiation amplitude (measured in electron volts) [16,18,19]. The amplitude results from constructive interference (in-phase) of returning waves from both the fixed and moveable mirrors, whereas destructive interference (out-of-phase) produces waves with zero amplitude. As depicted in Figure 1, the reflected rays penetrate the sample, absorb a portion of it, and convey the remaining portion to the detectors for interpretation of molecular vibrations in the sample [16,18]. To attain diffraction-limited resolution in the objective lens, synchrotron radiation is used as a source of photons [11].

The detector can be made of deuterium triglycine sulfate (pyroelectric detector) or mercury cadmium telluride (photon detector) [17]. The interferogram is then decoded into specific frequencies (wavenumber) using Fourier mathematical transformation [20]. The ratio of the intensity of the sample with blank spectrum (P/Po) and sample thickness (w) gives the transmittance (T).

As demonstrated in Equations (1)–(3) [21], the transmittance (T) can be represented as a function of the absorption coefficient (α_{abs}), and if inverted and transformed to logarithmic values, it becomes the absorbance (A):

$$T = \frac{I}{I_o} = e^{-\alpha_{abs}} .w \quad (1)$$

$$\alpha_{abs} = \log l - \log T \quad (2)$$

where I is the incident light intensity and lo is the transmitted light beam. For weakly absorbing homogeneous samples with known molar absorptivity (γ) and concentration (c), absorbance (A) can be stated as follows:

$$A = -\log T = \gamma.c.\ w \quad (3)$$

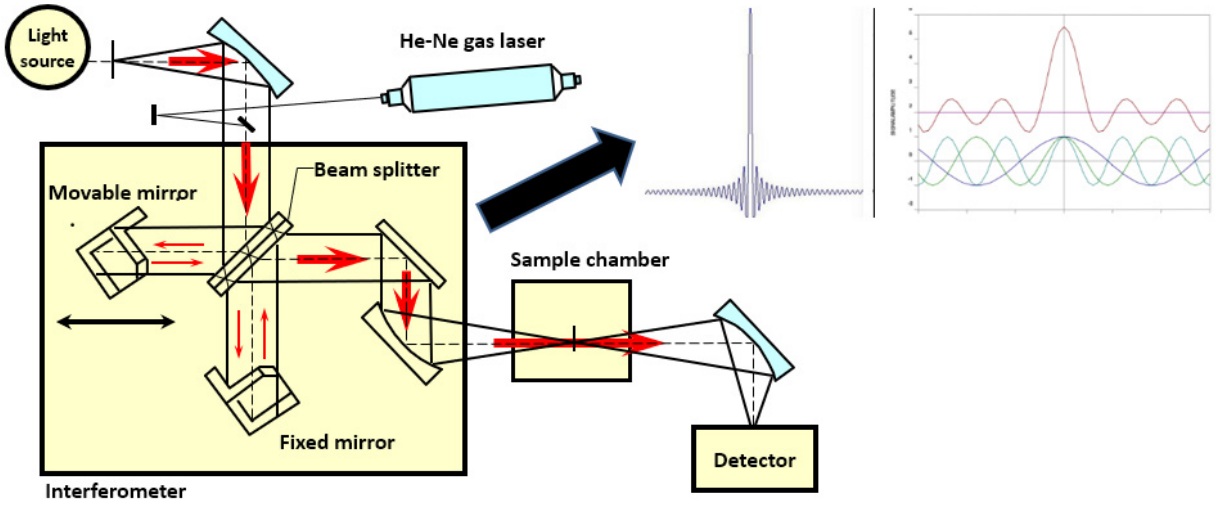


Figure 1. Mechanism of FTIR Interferometer (Ref. [16] and used under copyright permission through http://delloyd.50megs.com/newfolder/copyright.html, accessed on 3 December 2022).

1.3. Molecular Bond Vibrations

During the vibration of the molecule, the net change in dipole moment in a molecule occurs, thereby resulting in IR absorption [22]. In other words, the vibration of molecules initiates a fluctuation in its dipole moment and causes an interaction in the electric field that associates with radiation [8]. Depending on the degree of freedom, function energy falls into two principal categories (symmetry and asymmetry) and bending (rocking, scissoring, wagging, and twisting) [21], as shown in Figure 2. It requires more energy to stretch than to bend molecular bonds while slightly more energy is required to asymmetrically move atoms than symmetrically [10,23]. Therefore, bonds vibrate asymmetrically at a higher frequency than their bending. Additionally, the bond between hydrogen and oxygen atoms has been reported to have a higher frequency than heavier atoms. Similarly, the double bond atom has a heavier vibration than a single bond [23].

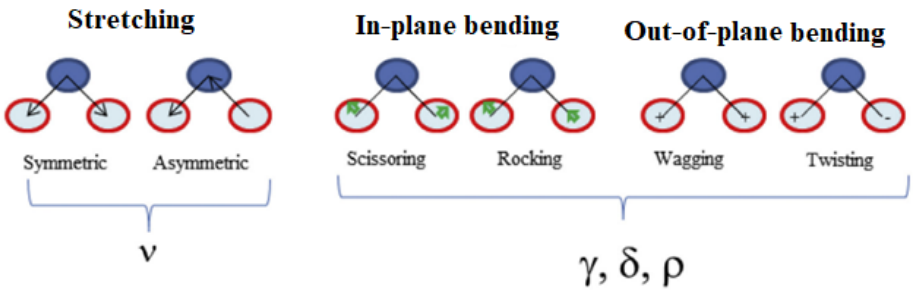


Figure 2. Vibration modes in FTIR spectroscopy "(From Ref. [21] and used under Creative Commons CC-BY license.)".

1.4. Sampling Methods in FTIR

FTIR spectroscopy can be conducted through different mechanisms of sampling methods, namely the transmission or reflection method, which can be attenuated total reflectance

(ATR) and the diffusive reflectance IR transmittance spectroscopy technique (DRIFTS) [24], and the specular aperture grazing angle (SAGA) methods [14,25].

1.4.1. Transmission Method

This method is convenient and simple and relied on the idea of light passing through a surface through a process of passing IR radiation through a thin, free-standing film with a thickness of fewer than 50 microns, thereby making it suitable for liquid, solid, and gas applications. The sample preparation by direct transmission could be difficult as it requires mixing the sample with a reference substance for quantitative analysis. To create a pellet, mull, or film, the sample would be combined with KBr in a volume ratio of 1 to 10 [15]. The method was utilized by Brown et al. [26] in 1958 to create a translucent disk before conducting the test. Likewise, Yu et al. [27] also added a sample to KBr blank ratio in one hundredth (weight). Yusuf et al. [28–31] studied bond characteristics in alkaline-activated palm oil fuel ash and also employed the KBr to sample ratio of 1:9 (by volume). Atta et al. [32] made use of kaolin and rice husk ash as precursors but reduced the sample/KBr volume ratio to 1:5. The prepared sample is then compressed using a hydraulic press (10 MPa) into a thin clear pellet before being placed into the radiation absorption device. After absorbing some energy, the sample delivers the remaining energy to the detector. The sample surface area, which can be increased by grinding the sample to a fineness below 2–5 microns, determines the increase in transmittance and resolution of the absorption bands [15,33]. To prevent cracking or shattering of the translucent disc, the sample must be gently inserted into the holder.

For cementitious material application, the transmission method is commonly used as the samples are well-prepared into a paste and then properly cured for a specific period. The sample should be adequately dried and then ground into a finely divided powder through a mortar and pestle before being pressed into a pellet by using a mold at a pressure of about 10 MPa to make it translucent. Grinding the sample into a finely divided powder reduces distortion of the absorption band and scattering losses, while a wet sample that is not properly dried will produce a broad peak with poor resolution. KBr should be well covered to prevent attracting moisture because it is a hygroscopic substance.

1.4.2. Reflection Methods

All samples can be processed through transmission technique in which light waves is directly sent through the sample. Reflection methods, however, requires simple sample preparation and it can be either through internal reflection spectroscopy (attenuated transmission technique, ATR) or external reflection spectroscopy (specular reflection) for smooth and reflective surfaces. It can also be the combination of both internal and external reflections such as in diffusion reflection IR spectroscopy (DRIFTS) for rough surfaces [34].

a. The Attenuate transmission reflection (ATR) technique:

ATR was introduced in the 1960's but now being popular used due to its easier sample preparation. It can be used for qualitative and quantitative analyses of both liquid and solid gel coating samples in accordance with ASTM C494 Section 18.1.2 [35]. Its principle is based on internal reflection of light wave through air/sample, solid/sample or liquid/sample interfaces [36]. It was recently shown that attenuated total reflectance FTIR (ATR-FTIR) spectroscopy could be used for the detailed analysis of hardened fly ash GP [36] or to study pore characteristics or carbonation effect. On this premise, Nedeljkovi et al. [37] use this method to investigate the effect of natural carbonation on the pore structure and elastic modulus of the alkali-activated fly ash and slag pastes. The tested sample is placed in a reflective medium composed of a crystal (such as a diamond) with a high refractive index (usually greater than 2) [24]. Information is collected in internal reflection from the surface or thin layer by external reflection.

Other materials could also be zinc selenide (ZnSe), germanium (Ge), and silicon (Si), with a higher refractive index and varying hardness and depth of penetration. ZnSe is not recommended for strong acid or base samples due to the possibility of surface

erosion by the formation of zinc complexes. Rather, water insoluble AMTIR crystals made from germanium, arsenic, and selenium with similar refractive indices are preferred [38]. The crystal generates an exponentially decaying wave (evanescent wave) that projects orthogonally onto the sample [22]. IR is directed into a crystal or an internally reflected element (IRE) of a relatively higher refractive index and then absorbs a portion of the energy of an evanescent wave and transmits the rest to reach the detector [39]. The greater the depth of penetration (path length) onto the sample, the greater the wavelength of IR [38]. The advantage of this technique is that a spectrum can be generated with easy sample preparation by just placing the core sample on the holder and screwing it tightly to receive the radiation.

b. Specular reflectance technique

This requires the sample to be reflective or be on a reflective surface while the required information is collected through a thin layer as it involves externally reflection of incident light waves.

c. Diffuse reflectance IR transmittance spectroscopy (DRIFTS) method

The method has the advantage of higher resolution with no rigorous sample preparation, like the transmission method [24]. The sampling technique is through powder samples without any prior preparation. The sample is added to the sample holder and information is collected in internal reflection from the bulk of the matrix. The reflection of the light depends on the transmitted and reflected quantities by the sample and that also depends on the material bulk properties. The reflected rays are collected with an ellipsoid or paraboloid mirror, while KBR could be used to dilute any absorbent materials. The parameters being analyzed include compactness, shapes, reflectivity, refractive index, and absorption of the particles. The sample should be well-ground and fine to ensure that the wavelength of incident light is bigger than its particles. This is necessary to minimize Mie scattering [40]. They [40] reported that both transmission and ATR are closer in accuracy but at a disparity with the DRIFTS method [24]. The best and appropriate technique depends on the type of application, the nature of the material, and its surface roughness.

For civil engineering applications involving bond characteristics, both transmission and ATR methods are commonly used due to their close accuracy [24]. It should be noted that the sample must be properly dried to enhance the sharpness of the spectra, as the presence of water will affect the accuracy of the data by blinding other signals due to water molecule strong bands [41]. To conduct this test, it is best practice to separate the binders from siliceous aggregates to avoid misinterpreting the Si-O bands in aluminosilicate or CSH binders. However, siliceous aggregate compositions could be studied separately if that is the research focus. Generally, paste samples should be dried without containing free (unbound) water to avoid blinding the relevant peaks of interest in the FTIR spectra. There have been several efforts by different researchers to solve the problem of the effect of moisture fluctuation on the spectra peaks. The problem is the presence of moisture that causes the fluctuation of temperature on the laser (He Ne), and of transient concentration of moisture along the spectrometer's light path. In recent time, Zhang et al. developed an approach to resolving the problem by using a comprehensive 2D-COS method [42]. Giordanengo et al. [43] proposed a holistic calibration and external parameter orthogonalization (EPO) among the effective approaches to remove additive and multiplicative effects of water on the vibration of -OH chemical bonds.

1.5. Factors Affecting Bond Vibrations

The molecules could vibrate whenever there is an energy level difference [44]. Change in molecular energy (ΔE) shown in Equation (4) is defined as the product of Planck's constant (h = 6.63 $\times 10^{-34}$ $m^2 \frac{kg}{s}$) and frequency of the normal mode (f = velocity(c)/ wavelength (λ)):

$$\Delta E = hv \quad (4)$$

Many factors affect the position or characteristics of the absorption band, which include the strength or stiffness of the bond between two adjacent atoms (k), which invariably depends on the valency of atoms and increases across the period, the square root of atomic weight (μ), and the coordination number of cations (CN) [1,44]. Further, the lighter the masses of the atoms and the stiffer the bonds, the higher the frequency of the vibrations (wavenumbers) of the molecules attached to the bond (Equations (2)) [45]. According to Keller et al. [15], from Hooke's law, the frequency of the absorption band (v) can be given in terms of the reduced mass (u) and unique chemical bond constant (k), as shown in Equation (5).

$$v = \frac{1}{2\pi}\sqrt{\frac{k}{u}} \tag{5}$$

With wavenumber, $\overline{v}$ = v /speed of light (c), and Avogadro number (N), Equations (6) and (7) become:

$$\overline{v} = \frac{1}{2\pi c}\sqrt{\frac{k}{\left(\frac{u}{N}\right)}} \tag{6}$$

For $h_c = 3 \times 10^{10} \frac{cm}{s}$ and Avogadro's number, $N = 6.02 \times 10^{23}$:

$$\overline{v} = 4.12\sqrt{\frac{k}{u}} \tag{7}$$

where $u = \frac{m_1 m_2}{m_1 + m_2}$ is the reduced mass (g/mol) of the two vibrating atoms of masses, m_1 and m_2, N is Avogadro's number, c is the speed of light, and k (dyne/cm) is the unique chemical bond force constant which increases with the number of π bond within the molecules such that triple, double, and single bonds have the values of 1,500,000, 1,000,000, and 500,000 dyne/cm, respectively.

2. Historical Background of the Utilization of FTIR for Bond Characterization in Cementitious Binders

Ordinary Portland cement, alkaline-activated slag (AAS), and geopolymer- or alkaline-activation of aluminosilicate materials, such as class F flyash, metakaolin, and others, may be used as cementitious binders for civil engineering applications [25,46,47]. Material science was one of the earliest applications of FTIR technology. Researchers in structural materials, civil engineering, and cement chemistry have been attempting to comprehend the skeletal framework of this binder, which is primarily composed of inorganic silica and alumina, for qualitative evaluation.

On this note, Hunt et al. [48] were one of the first researchers to use FTIR to characterize inorganic minerals with wavelengths ranging from 2 to 16 microns. They reported the possible application of the method to soil and ceramics before [49] and used it to study silicate structures. Afremow [22] used IR spectroscopy to investigate inorganic extenders and pigment in the mid-IR region of 200–1500 cm^{-1} in 1966 in an effort to comprehend their properties. To aid in the interpretation of spectra, Nakamoto [50] created an atlas of inorganic, organometallic, bioinorganic, and coordination compounds. As early as 1978, the technique was also utilized in various areas of material science, most notably in the characterization of clay minerals, such as illite and montmorillonite [44]. In addition, they distinguished kaolinite (doublet peak), halloysite (singlet peak), and nontronite (singlet peak) (no peak). The shifting in the spectral band distinguished montmorillonite, illite, and muscovite, which had the highest K_2O, based on their respective wavelengths of 9.35, 9.7, and 9.6 microns.

The application of FTIR directly to the analysis of cementitious binders began in the early 1970s. Based on this premise, Bensted used infrared (IR) and Raman techniques to identify the phases of OPC binders in 1974 [51,52], and Laser–Raman techniques were used to identify these phases in 1976 [24]. He asserted that the wavenumber used to characterize solid minerals, such that clay spectrum was found within the mid-IR wavenumber range

of 400 to 4000 cm^{-1}, which corresponds to a wavelength range of 2.5 to 25 μm [9]. In 1980, Ghosh and Handoo [53] successfully identified ettringite, monosulfate phases, and the efficacy of admixture during the cement hydration process. In addition, they asserted that the identification of rock minerals during the production of OPC cement and cement quality control could be accomplished qualitatively with the aid of FTIR and that the identification of reactive siliceous aggregates or mineral rock could be accomplished quickly. In addition, they discovered phases of mineral present in anhydrous OPC, which include alite (925, 885−895, and 520 and 465 cm^{-1}), belite (965−985 cm^{-1} and 845−850 cm^{-1}), gypsum (1080−1100 cm^{-1}), tetracalcium aluminoferrite (720 cm^{-1}), and tricalcium aluminate (Figure 3).

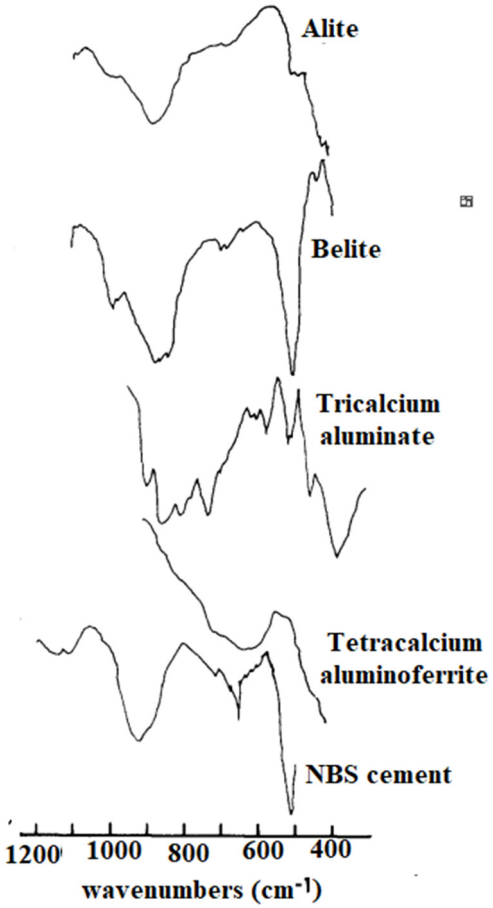


Figure 3. FTIR spectra of anhydrous cement phases (From Elsevier Ref. [53] and used with permission).

In 1982, Stolper [54] asserted that it would be possible to determine the hydroxyl ion group concentration and molecular water in the already-cooled melted silicate. Moreover, cement contains various cations such as Ca^{2+}, Na^{+}, K^{+}, and radicals which include $-OH^{-}$ (portlandite), SO_4^{2-} (gypsum), silicon oxides (SiO_2), and alumina (Al_2O_3). The prominent compounds in OPC are alite (C_3S), belite (C_2S), tricalcium aluminate, (C_3A), and tetracalcium aluminoferrite (C_4AF). They were formed through covalent bonding of minerals and oxides.

Alkaline-activated binders (AABs) and geopolymers (GPs) are composed of precursors and activators (alkalis and water glass), which are activated by room or thermal curing [55,56] through the processes of dissolution, transportation, and condensation before forming the aluminosilicate network of sialates [6,28]. To understand the bond characteristics of aluminosilicate and zeolite networks, Bartholomew et al. [57] applied IR spectra to investigate the vibration of water glass (N_2O-K_2O-ZnO-Al_2O_3-SiO_2) in 11% of

water within a fundamental and overtone band of 1.41–6.1 μm. Through this effort, molar absorptivity was determined for a hydrated glass for water and hydroxyl levels at a specific wavelength (2.22 μm). In 1982, William [58] in New York examined the performance of synchrotron radiation in comparison with a 2000-K black body source within the infrared region 1–100 μm, and it was reported that synchrotron light source was reported to be more effective at longer wavelengths than black body sources.

To understand the bonds that existed within silicate minerals, the insertion of oxygen within silicate bonds, and their reorganization, Mawhinney et al. [59] used FTIR to examine the vibration of Si -Si and Si-H and the effect of O penetration to form Si-O-Si and Si-OH, respectively. In 1999, Karakassides et al. [60] reported that silicon apical oxygen in asymmetric stretching underwent a significant change at higher temperatures in montmorillonite clay. With more understanding of silicate concatenation, Yu et al. [27] used the technique to distinguish different C-S-H in different zeolites that existed within cementitious binders (CB) based on their Ca/Si ratios. With a new insight into the vibration of H_2O and OH^- bands, they were able to distinguish between jennite, 1.4 nm tobermorite, and 1.1 nm tobermorite, while categorizing the main vibration peaks in the IR spectra as 950–1100, 810–830, 660–670, and 440–450 cm^{-1}.

Furthermore, in order to have a detailed understanding of stretching and bending vibrations in silicate, aluminate, carbonate, and hydroxyl-bonded molecules, King et al. [8] showed that asymmetric stretching for Al-O and Si-O existed within the mid-infrared and, therefore, assigned 1100 and 1210 cm^{-1} for asymmetric stretching of Si-O, just as 470 cm^{-1} was assigned to O-Si-O/Si-O-Si bending vibrations. They further characterized tetrahedral Al-O stretching bands existing within polymerized calcium aluminate ($CaAl_2O_4$) glass at 820 and 680 cm^{-1}, while Si-O bond vibrations in silica (SiO_2) were noted at 1100/1200 and 810 cm^{-1}. Additionally, O-Al-O/Al-O-Al had a detectable deformation mode at 425 cm^{-1}. Both Al-O and Si-O are very prominent modes in geopolymers and AABs, as they define the aluminosilicate framework that governs the strength characteristics. Since the strength of materials depends on their microstructural composition and framework, researchers began to study the strength performance through qualitative analysis of the silica and alumina bonds present in a CB.

Moreover, the bending of S-O could be noted at the band at 450, 600, and 680 cm^{-1}, while the stretching was reported to occur at 1080–1140 cm^{-1}. The possibility of noting S-O bonds in FTIR spectra has given the opportunity to study concrete durability and its setting time due to the presence of sulfate in ettringite (Aft) formation in OPC binders. Tararushkin et al. [61] reported that the strength of a binder will decrease with the formation of ettringite (S-O), noted via FTIR spectra. Similarly, the study of the carbonation of concrete paste due to environmental exposure can be corroborated by observing C-O spectra using FTIR. Further, CO_3^{2-} bending in-plane and out-of-plane were reported at wavenumbers 680–740 and 860–880 cm^{-1}, respectively, while stretching O-C-O in CO_3^{2-} and CO_2 were 1410–1510 and 2350–2390 cm^{-1}, respectively [62]. This provides adequate information for characterizing AAS and GP [5]. Many other researchers [63–65] investigated and reported on the qualitative durability of sodium and magnesium sulfate in 2005, and Ismail et al. [66] and Yusuf et al. [28] followed suit. FTIR was used to observe that there was more leaching of alkali in Na sulfate than observable in Mg sulfate [28,66].

Furthermore, the four main binders, which include Portland cement (PC), AAS, GP, and a mix of GP-AAS, were identified and characterized by the FTIR method by Lecomte et al. [63]. They asserted that C-S-H in OPC is semicrystalline, while AAS, GP, and AAS-GP are amorphous in nature. Due to this, it is quite difficult to completely distinguish various phases in AAB and GP by using X-ray diffraction (XRD) techniques. In 2006, Coates [10] published a review on the application of FTIR to organic compounds and adumbrated other various factors that could affect the vibrational frequencies of organic compounds—aromatic compounds, olefinic groups, and saturated aliphatic bonds. They also reported organic siloxane (Si-O-Si) at wavenumbers of 1095–1075/1055–1020 cm^{-1}.

Davidovits [6] published a book titled *Geopolymer Chemistry and Application* in 2008, where the chemistry of geopolymer binder was discussed in distinction from alkaline-activated binders and OPC. He also discussed the application of FTIR, XRD, and NMR for the characterization of cementitious binders, and subsequently wrote a specific review on the synthesis of Ca-based geopolymers or alkaline-activated slag (AAS) due to the proliferation of Ca-like compounds (calcium aluminosilicate hydrate (CASH)) present in ground granulated blast furnace slag (GGBFS) and Class C fly ash. It was established by both Lecomte et al. [63] and Davidovits [6] that FTIR could indicate the disparity between CASH, NASH, and CSH products in AAS, GP, and OPC, respectively.

In 2008, Garcia-Lodeiro [67] studied the disparity between CSH and NASH and asserted that depolymerization occurs due to a reduction in the pH of the binder. In another study, they incorporated Ca in the NASH binder and thereby noticed the impact of cation attachment on Si-O-Si bond vibration [45,65]. They attempted to understand the effects of alkali and aluminum in geopolymer binders [37], thereby establishing the fact that aluminum and alkali affected the AAS by increasing silicate polymerization. This points to the fact that FTIR could be used to determine the degree of aluminosilicate polymerization qualitatively and comparatively between different samples. Other instruments they used together with FTIR include TEM, EDX, and XRD. Different types of silicate chain structures (cyclic structures of siloxane, Si-O-Si) could be predicted through FTIR spectra [68].

In 2012, Fernandez-Carrasco et al. [23] identified two major broadband peaks for alite in OPC binders for symmetric and asymmetric stretching at 870 and 940 cm^{-1} due to vibration of the tetrahedral silicate unit (SiO_4), while symmetric and asymmetric bending were observed at 525 and 450 cm^{-1}, respectively. Belite (C_2S) was also noticed to have a silicate tetrahedral unit phase that vibrates with more energy within 800–1000 cm^{-1}, while bending vibration absorption bands were noticed at 520 cm^{-1} with a shoulder at 538 cm^{-1}. Additionally, tricalcium silicates (C_3A) were identified through Al-O_4 tetrahedral groups with two different peaks at 650–950 cm^{-1} and 380–500 cm^{-1}, respectively.

Other Al-O maxima peaks can be found near 820–900 cm^{-1} and 705–780 cm^{-1} for the tetrahedral (AlO_4) unit, and at 414–520 cm^{-1} for the octahedral (AlO_6) unit. The vibration peaks of calcium tetrahedra-aluminoferrite (C_4AF) due to stretching of [$(Fe,Al)O_4^{5-}$] were at a wavenumber range of 800–830 cm^{-1} with a maximum close to 720 cm^{-1}, while a less intense broad peak with several maximums at 620 and 670 cm^{-1} was also reported. Garcia-Lodeiro [69] further explored the characterization of alternative binders to CSH in traditional mortar and concrete production. They identified various factors affecting the activation of AAB, such as curing temperature, alkaline activators, and silica modulus or percentage compositions of SiO_2, Al_2O_3, and CaO. The mechanisms of framework and the silicate network of different binders for OPC, geopolymers, and alkaline activation were identified as CSH and NASH, respectively. However, using FTIR, the latter evolved into C-N-A-S-H and (C,N)-A-S-H. These products were observed to be distinctively different from CSH in an OPC binder.

Casale et al. [39] distinguished the quality of concrete produced from different admixtures and their combinations, which include air entrainers, accelerators, retarders, and water reducers, by using the correlation coefficient of an IR scan in accordance with ASTM C 494. This suggests that FTIR can identify the framework of aluminosilicate bonds in geopolymer products and linear chains of tobermorite gel in OPC binders [22]. Kiefer et al. [14] also identified FTIR to differentiate bonds existing within different radicals by showing how Na_2SO_4 and $CaSO_4$ could be identified differently. They also indicated the peaks and vibration modes for hydroxyl bonds (Si-OH) (3164–3630/1610–1630 cm^{-1}) [70], carbonates (702–715 cm^{-1}/866–878/1390–1420 cm^{-1}) [70], and sulfate with their crystallization water (658–668 cm^{-1} /triplet band, 1100–1160 cm^{-1}) [66]. This finding also aligns with Kramar et al.'s [71] ascription of the 1624 cm^{-1} wavenumber to water H-O-H or -OH molecule bending vibrations.

Generally, FTIR is being used for qualitative analysis for cementitious binders in civil engineering applications; however, there are ongoing efforts toward adapting to the

technique for quantitative analysis in material science and analytical chemistry with a view to knowing the amount or the concentration of the analyte in a sample relative to calibrated standards [72]. However, this is beyond the scope of this review.

2.1. FTIR Spectra of Si-O-, T-O, Si-O-T and the Degree of Crystallization and Polymerization

According to Afremow et al. [22] and Garcia-Lodeiro et al. [45], the asymmetric stretching (v_a) and bending (δ) of Si-O-T are between [830 and 1200 cm^{-1}] and [435 and 540 cm^{-1}], respectively. These absorption bands are crucial to the skeletal framework of OPC, geopolymers (GPs), alkaline-activated slag (AAS), and alkaline-activated binders (AABs) as cementitious binders [38]. All compounds contain -T-O (T=Si or Al) bonds, either in tetrahedral frames in geopolymers, or linear chains in the hydration product of hydraulic cement [46,63]. These peaks may provide information regarding the polymerization, crystallization, or amorphorsity of the binder, and in some cases, they may even indicate the binder's strength qualitatively. For instance, Yu et al. [27] asserted that the shallowness, narrowness, and sharpness of the Si-O-T band could indicate the crystallinity of the binder. This contrasts with the dome-like or smooth, curved nature of vitreous or amorphous aluminosilicate geopolymer substances. Lee et al. [3], Davidovits [6], and other researchers reported identical findings [63,67] because as the Ca/Si ratio increases, the product becomes more crystalline, while polymerization decreases due to its shorter chain length. Chen et al. [73] reported that jennite (Ca/Si = 1.5) has a higher degree of crystallinity than 1.4 nm-tobermorite (Ca/Si = 0.83). This observation is consistent with that of Garcia-Lodeiro [74], who identified two systems, G1A (Ca/Si = 1.2) and G2B (Ca/Si = 1.9), as depicted in Figure 4, in which lower Ca/Si ratios indicate more degrees of polymerization due to a higher frequency of vibration, as indicated by a greater wavenumber.

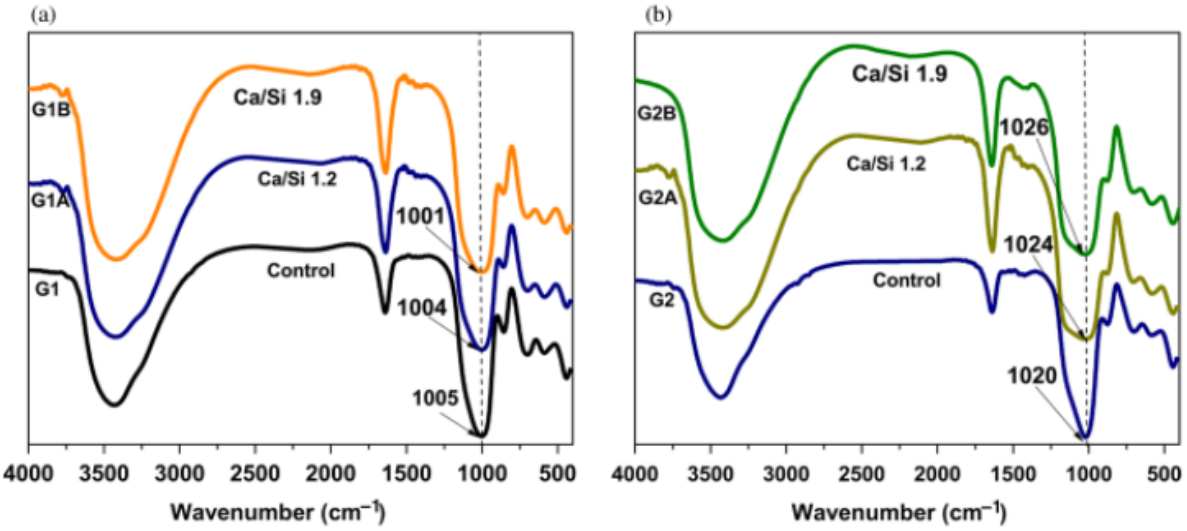


Figure 4. Aluminosilicate (Si-O-T) band due to an increment in C/S ratios (**a**) Si/Al = 1 and (**b**) Si/Al = 2 (From Wiley Ref. [74] with copyright permission).

However, the presence of alumina within the binder could increase polymerization due to the bonding of Al with Si-O to form additional Si-O-Al bonds within the framework. Si/Al = 2 promotes more polymerization of the aluminosilicate bond than Si/Al = 1, as evidenced by the broader mid-IR bands at 1004 to 1024 cm^{-1} (Ca/Si = 1.2) and 1001 to 1028 cm^{-1} (Ca/Si = 1.9) [45]. According to Lecomte et al. [67], the degree of polymerization increases with the attachment of tetrahedral Al ions to silica in IV-fold coordination to form aluminosilicate bonds [45,63].

The Si/Al ratio decreases due to an increase in Al incorporation (Si-O-Al), whereas the Ca/Si ratio rises due to Ca attachment to the silica chain. The increase in absorption band frequency is a result of the high silicate organization that accompanied the low presence of

Al within silicate (Si-O-Si) chains. The Si-O bond in the linear silicate chain of OPC is less polymerized, as shown in Figure 5.

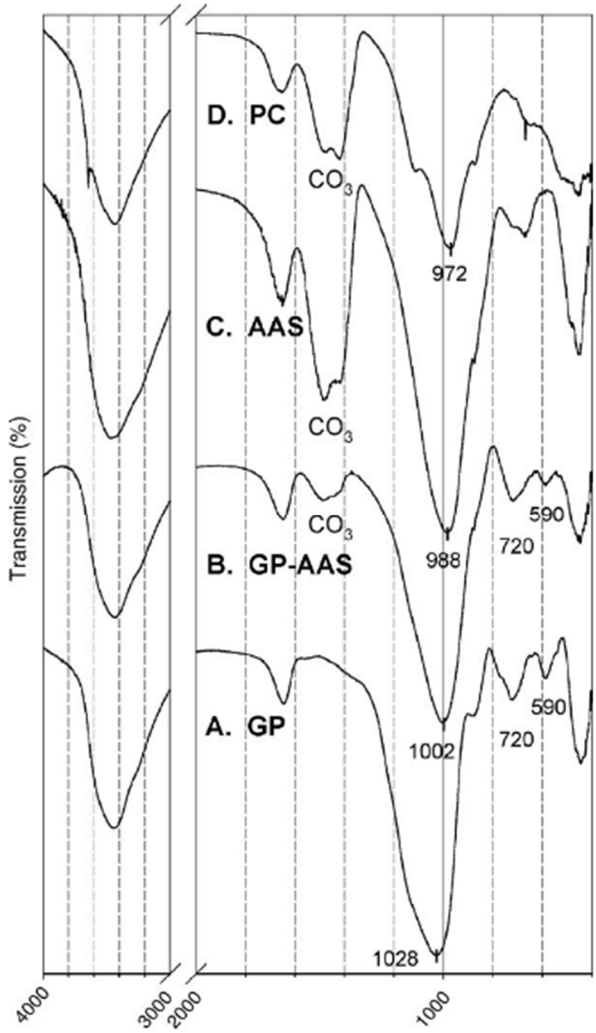


Figure 5. Vibration bands in OPC, AAS, and geopolymer binders (From Elsevier Ref. [63] and used with copyright permission).

Consequently, the asymmetric stretching of this band was measured to be 972 cm^{-1}. Due to the overlap of Si-O with Ca(Si-O-Al) and Ca(Si-O-H) bands, the peak is less broad compared to AAS and GP synthesis, whose peaks are not only broad but also prolonged with higher value wavenumbers at 988 and 1028 cm^{-1}, respectively. This suggests that the material is less amorphous. Rovnaník [75,76] made the same observation when comparing the effects of C12A7 on a fly ash GP binder, where it is reported that tetrahedra alumina enhances binder polymerization by attaching to the Si-O chain. In other words, the degree of polymerization due to silicate concatenation increases with the silica modulus. Lee et al. [3] and Lecomte et al. [63] observed that Al incorporation in Si-O-Si influences the order of polymerization and chain formation of the silicate framework. A crystalline binder could be identified by the narrowness and depth of the Si-O-T band (where T is either Si or Al) in the wavenumber range 850–950 cm^{-1}, whereas the broader band around 3300–3650 cm^{-1} indicates the concentrations of hydroxyl ion and water molecules. In addition, Gougazeh and Buhl [77] found that the concentration of hydroxyl ions and the silica modulus (SiO_2/Na_2O) ratio could affect the degree of polymerization and crystallinity of the binder.

The polymerized GP product has a deeper and wider band trough than Portland cement (PC) and AAS binders [63]. The substitution of Si in Si-O-Si with the more electronegative Al^{3+} led to a longer polymerized chain (Si-O-Al). FTIR could detect an increase in silicate reorganization as a result of the formation of longer chains, as observed in the system (Si/Al = 2) and in geopolymer synthesis [6]. Therefore, the process of product formation in Al-rich precursors, such as metakaolin, may differ from that in calcium silicate (Si-rich gel) dominant types, such as AAS. According to Figure 6 [77], an excess of alkali in the mixture increases the dissolution, causing the silica bond to break. This results in the replacement of the terminal hydroxyl ion with cations, which inhibits the polymerization of the binder. Therefore, the lower the concentration of alkaline, the lower the proliferation of terminal hydroxyls that result in chain discontinuity (lower polymerization).

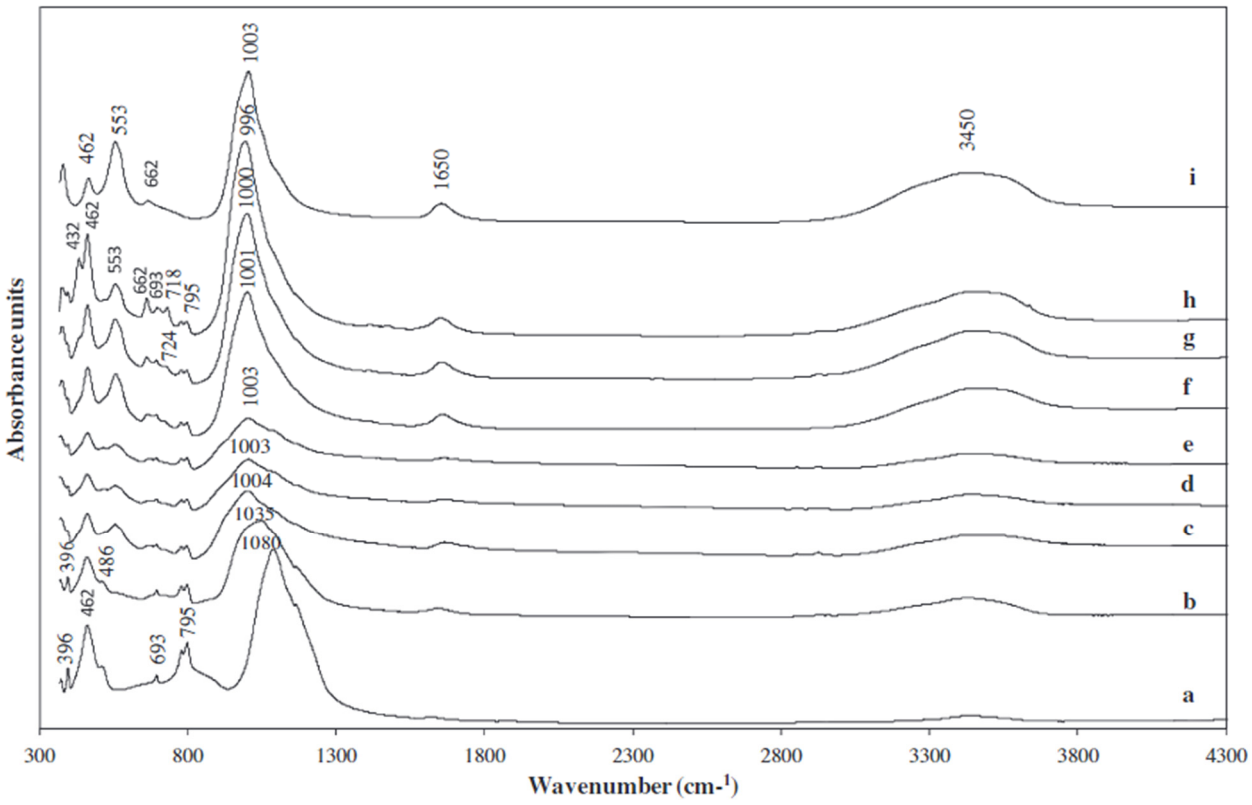


Figure 6. FTIR spectra of zeolite **A** and associated phases obtained by hydrothermal synthesis: (a) unreacted metakaolin, (b) 1.0M NaOH, (c) 1.5M NaOH, (d) 2.0M NaOH, (e) 2.5M NaOH, (f) 3.0M NaOH, (g) 3.5M NaOH, (h) 4.0M NaOH, and (i) commercial zeolite A (Fluka No. 69836) (From JAAUBA Ref. [77] and used under Creative Commons CC-BY license).

Due to the presence of a lower terminal hydroxyl, it appears that the Si-O-Si bond polymerizes more at lower alkaline concentrations. A lower concentration of alkali (hydroxyl ions) results in a lower Na/Si or Ca/Si ratio, which increases the amorphousness of the products. The Si-O-Si band stretches at 1080 cm^{-1} in a sample of mild alkali (1.0 M NaOH) compared to 996 cm^{-1} in a solution with a higher concentration (4 M NaOH) [77]. As evidenced by the disparity between a and h, increasing the Ca/Si ratio and hydrogen bonding from adjacent hydroxyl will increase the crystallinity of the product. The crystallinity of hydrogen bonds distinguishes jennite from tobermorite.

These results are consistent with Kramar and Ducman's [71] findings, as well as the correlation between the degree of geopolymerization and the frequency of vibration, which decreases from 1078 to 1015 cm^{-1} as the amount of Al-O incorporated into the Si-O bond increases. They also assigned the wavenumber 1624 cm^{-1} to the water H-O-H or -OH molecule's bending vibrations. Other researchers [78] indicated that the peaks and vibration

modes for hydroxyl bonds attached to silica (Si-OH) would have peaks between 3164–3745 and 1610–1630 cm^{-1}. It is evident that FTIR could be used to distinguish amorphous and semi-crystalline samples through observation of Si-O-T bond vibrations.

2.2. The Effect of Silica Modulus, Alkali, and Aluminium on Si-O-T and T-O Vibrations of FTIR

In cementitious binders, the vibrations of T-O and Si-O-T are crucial. Lecomte et al. [63] found that a Si-O-T bending vibration around 450–500 cm^{-1} is more pronounced in GP-A than in the 1.4 nm tobermorite of the shorter chain in (OPC-D) (Figure 5). As shown in Figure 6, as the concentrations of alkalis (OH^- and Na_2O) increase, the Si-O-T bands become narrower. The formation of zeolites or aluminosilicate chains increases as the silica modulus (SiO_2/Na_2O) increases to 0.69 [79]. Spectra (N) were activated by NaOH, whereas W15 required a combination of Na_2SiO_4 and NaOH (Figure 7). The higher Na_2O content narrows the Si-O-T band, whereas the addition of silica increases its degree of polymerization, as indicated by W50 (1020 cm^{-1}) in comparison with N (1000 cm^{-1}).

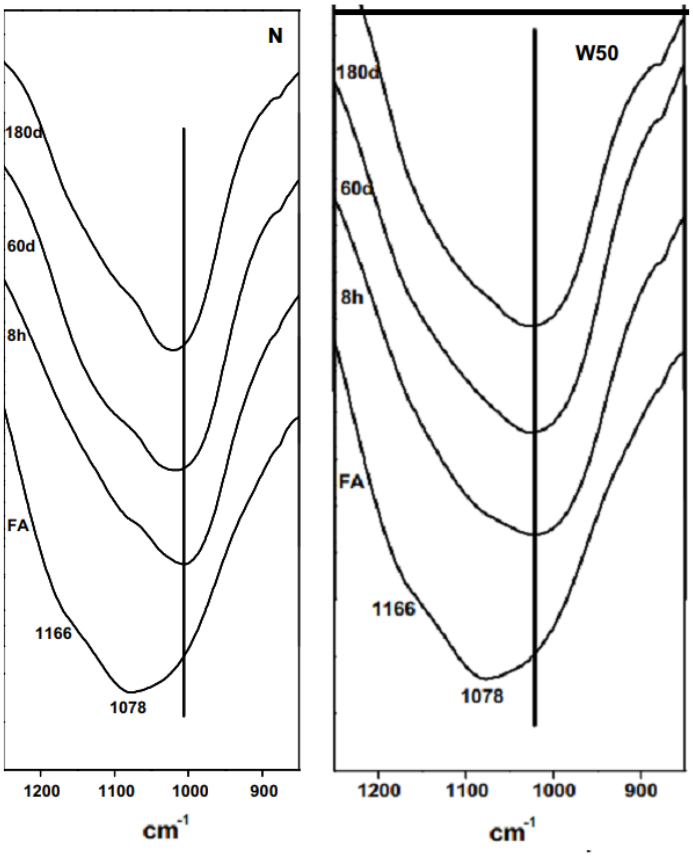


Figure 7. Si-O-T asymmetric vibration band with silica modulus, N-NaOH activator, and both ($NaOH+Na_2SiO_3$) in W50 such that Na_2O/SiO_2 = 0.69 (From Elsevier Ref. [79] and used with copyright permission).

El-Didamony et al. [80] reported a spectrum band at 988 cm^{-1} assigned to the orthosilica unit $[Si_2O_7]^{6-}$, in which partial substitution of Al^{3+} for Si^{4+} is possible. Gougazeh and Buhl [77], along with Ghosh and Handoo [53], assigned the bending vibration of Si-O-T to the range 400–520 cm^{-1}, whereas Criado et al. [81] reported the distinction in the Si-O-T band in fly ash GP due to the varying proportion of silica modulus (SiO_2/Na_2O) in the alkaline activators. Fernandez-Carrasco et al. [23] also reported that the Si-O-Si stretching vibration within the layers of CSH gels overlaps with the gypsum S-O vibration within the bands 890–955 cm^{-1}.

In addition, symmetric stretching of the tetrahedral unit of Si-O and Al-O was centered between 890 and 955 cm^{-1}, whereas asymmetric stretching was observed between 870 and 940 cm^{-1} (Figure 8) [58]. The O-Si-O bonds stretch symmetrically and asymmetrically at 450–525 cm^{-1} for antisymmetric and symmetric bending, respectively, while the Si-O-Si bonds stretch between 800 and 10 cm^{-1}. Si-O elongation oscillates between 840–990 and 840 cm^{-1}, whereas bending vibrates between 520–538 cm^{-1}. The vibrations of tetrahedral Al-O (AlO_4) induced by ettringite (Aft) formation were detected at wavenumbers of 705–820 cm^{-1}, while octahedral (AlO_6) was at 510–520 cm^{-1} and 414–460 cm^{-1} [58].

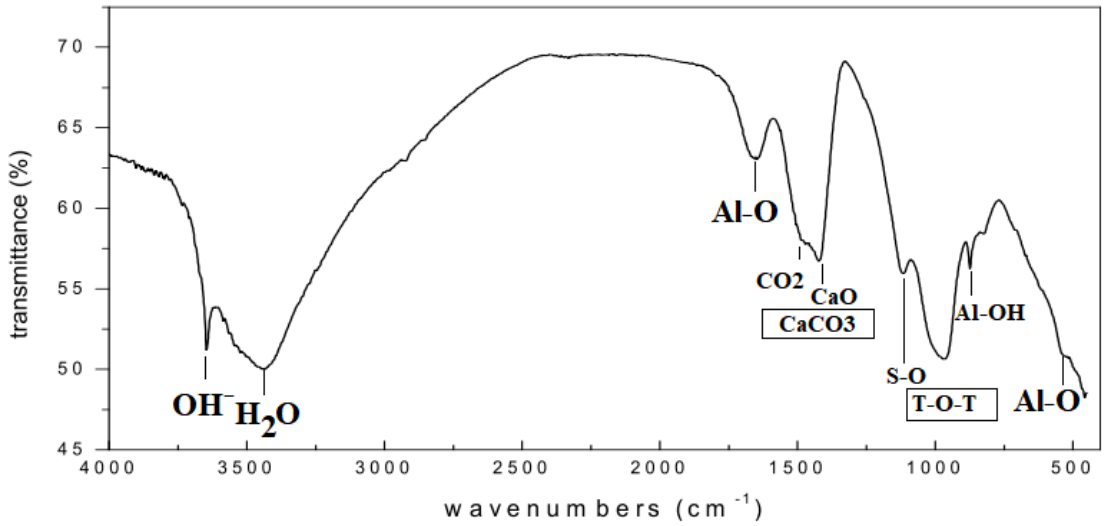


Figure 8. FTIR spectra in ordinary Portlandite cement (From IntechOpen Ref. [58] and used under Creative Commons CC-BY license).

The Si-O-T asymmetric stretching vibration can also be detected in FTIR spectra at the wavenumber range of 1116–1148 cm^{-1} for an unreacted phase in rice husk ash (RHA) and metakaolin (MK) precursor [32], whereas the Si-O-T bending vibration was noted within 520–550 cm^{-1} for an unreacted phase in OPC. El-Didamony et al. [80] attributed these asymmetric stretching and bending bands of Si-O-T to gehlenites (CASH-($Ca_2Al[AlSiO_7]$) and akermanite (CMSH-$Ca_2Mg[Si_2O_7]$) within the mellinite framework of blast furnace slag. Karakassides et al. [60] also detected symmetric stretching of Si-O-T bridges between 671 and 717 cm^{-1}. Garcia-Lodeiro et al. [65] also identified symmetric stretching of silica gel (Q^2 unit) with a wavenumber of 815 cm^{-1} and asymmetric stretching with a lower degree of polymerization at 970 cm^{-1}.

Similarly, the concentration of NaOH could affect aluminum (Al) substitution in alkaline binders due to more dissolution that causes freer Si-O and Al-O monomers to be available prior to the condensation to form oligomers [31,81–83]. The presence of a higher concentration of alkali in a geopolymer will reduce the amorphousity of the sample and the frequency of vibration increases as the polymerization of Si-O-Si increases [37]. This assertion is very important when analyzing the GP or AAB by using the FTIR technique. The frequency of vibration of Si-O-Al is lower when an activator containing a higher concentration of NaOH or a substance with a higher pH is used. Rees et al. [36] reported that the presence of a silicate monomer could affect the Si/Al ratio and stretching vibration of the Si-O-Al bond in infrared. In addition, they identified Al-rich gel as the intermediate formation preceding the final gel deposition. However, the duration depends on the concentration and speciation of the silicate. Fernandez-Jimenez et al. [84] support this claim in the classification and identification of GP.

Concerning the reactivity of Al, Yusuf et al. [30,31] infused $Al(OH)_3$ into alkaline-activated ground blast furnace slag in synergy with ultrafine palm oil fuel ash (AAGU) (Figure 9) and observed an improvement in the amorphorsity of the product, as indicated

by the Si-O-T (T=Si or Al) band elongation. The hydroxyl component was observed to reduce the degree of polymerization. Hajimohammadi et al. [85] demonstrated via FTIR spectroscopy that the rate of release of Al to form C/N-A-S-H in the Si-O-T vibration band is dependent on the source of alumina, with a slower rate observed in an inorganic source from sodium aluminate (952 cm^{-1}) compared to amorphous Al (964 cm^{-1}) synthesized via the Sims and Bingham methods.

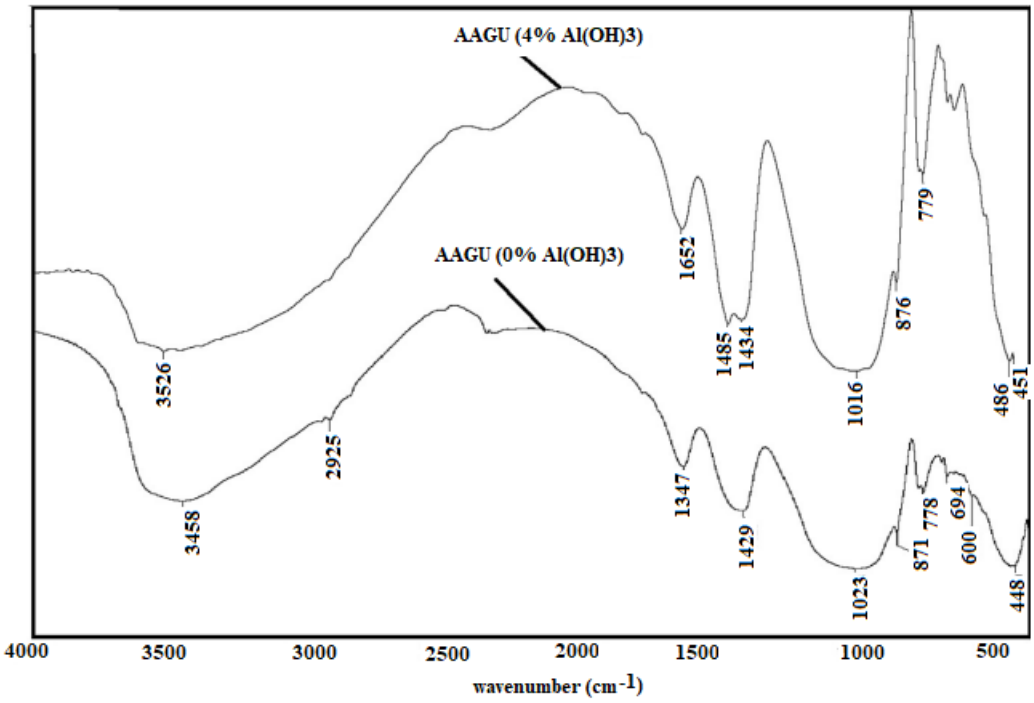


Figure 9. The effect of Al on Si-O-T band asymmetric stretching in an alkaline binder (From Elsevier Ref. [30] and used with permission).

Dealumination (the removal of Al from Si-O-T) by acidic attack or other processes could also increase this specific vibration band, as reported by Bakharev et al. [86]. Yusuf et al. [30] in their study (Figure 9) showed that the introduction of $Al(OH)_3$ powder into the AAB causes changes in the asymmetric stretching of Si-O-Al from 1023 cm^{-1} to 1016.3 cm^{-1}. The important bands used to study the performance of materials are observed in Si-O and Al-O vibrations, such that the incorporation of Al causes asymmetric stretching to reduce the frequency from 1023 to 1016.3 cm^{-1} [87]. Clayden et al. [87] also identified spectra band 600–800 cm^{-1} to Al-O in IV-fold coordination with a SiO_4 atom in the bending mode. Taylor 1990 [88] also suggested the assignment of band 700 cm^{-1} to indicate the substitution of more reactive tetrahedra alumina (AlO_4) than its octahedral linkage (AlO_6) within the silica network at a spectrum band of 620 cm^{-1}. Brindley et al. [89] asserted that the preponderance of AlO_4 (IV) in metakaolin (MK) remarkably differentiates it from kaolinite minerals, which have excess Al (VI).

This implies that aluminate in IV-fold coordination, such as that found in metakaolin and class F flyash, is more reactive and beneficial to cementitious binders when used as base materials for GP synthesis [90,91]. Atta et al. [32] also assigned wavenumber 452 cm^{-1} with the T-O bending vibration of AlO_4. Garcia-Lodeiro et al. [69] validated the role played by Al in the process of GP polymerization by adding aluminum nitrate ($Al(NO_3)_3$) to C-S-H, which increased the vibration of the Si-O-T bond. This signals an improvement in the amorphorsity of the product (Figure 10) [45,74]. NA2 and NA4 that contained $Al(NO_3)_3$ showed a broader peak between 900–1100 cm^{-1} compared to the lesser frequency noted in the aluminate-free control sample (NC control). The amorphousness of the product increased due to the penetration of Al within Si-O-Si, thereby making the band

1000–1200 cm^{-1} deeper and broader as the SiO_2/Al_2O_3 ratio becomes lower. More silicate concatenation in the aluminosilicate framework is noted in the presence of higher (N10) and lower (N2) concentrations of alkali (Figure 11) [45].

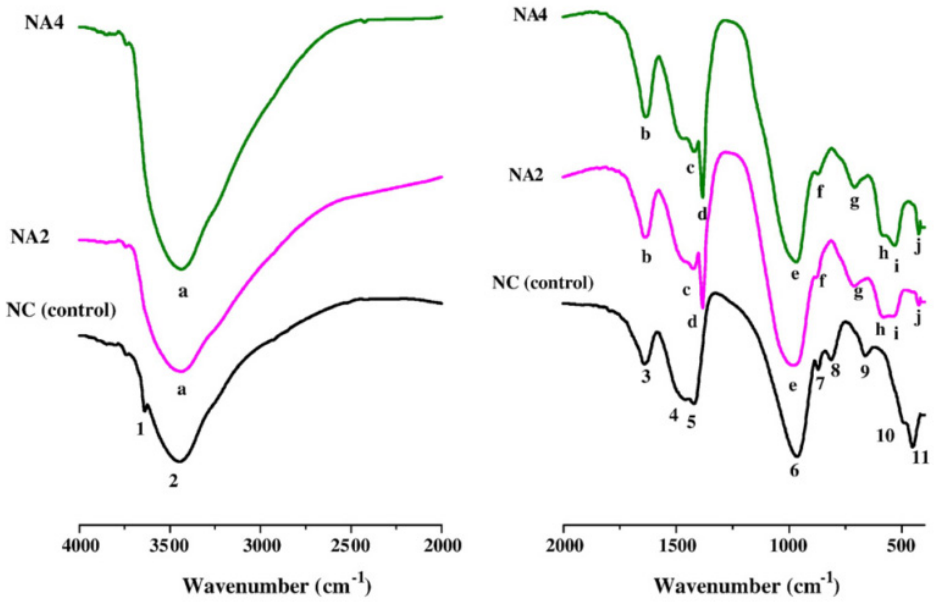


Figure 10. The role of aluminum in the asymmetric stretching of Si-O-T (in NC, NA2, and NA4 containing $Al(NO_3)_3$). From Elsevier Ref. [65] and used with permission.

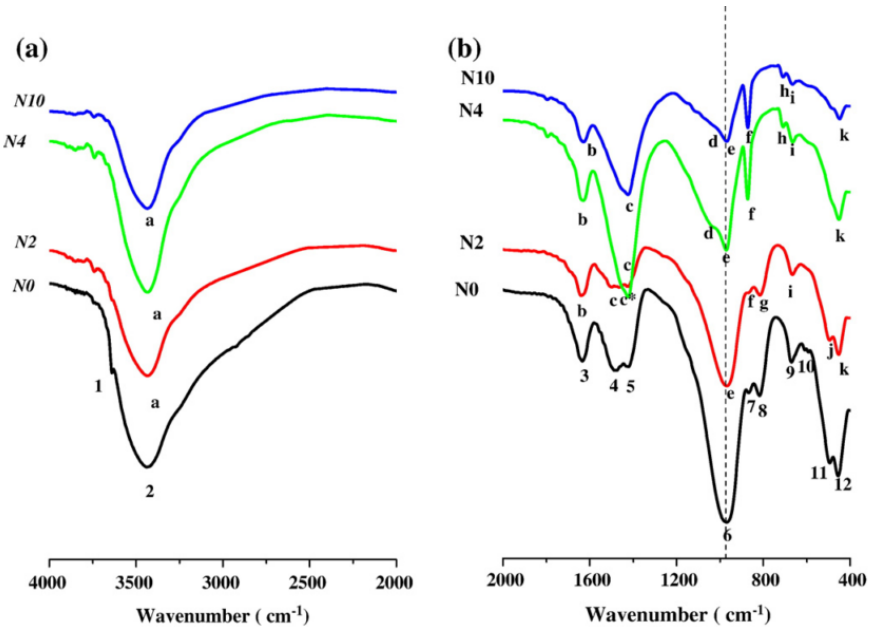


Figure 11. The effect of NiO_2/SiO_2 on Si-O-T asymmetric vibrations in FTIR for (**a**) OH/HOH and (**b**) Si-O-T bands (From ACS Ref. [45] and used with permission).

2.3. Analyses of CO_3^{2-} Vibration in FTIR Spectra

Several researchers have used FTIR to determine the level of carbonation and to qualitatively distinguish between different samples. Nedeljkovic et al. [37] identified asymmetric stretching (v^3), out-of-plane (v^2), and in-plane bending of CO at 1471 cm^{-1}, 856 cm^{-1}, and 715 cm^{-1}, respectively. These identified bands are assigned to calcium carbonates, calcite, and aragonites, respectively [91,92]. The vibration of linear C-O bond from calcite

($CaCO_3$) could be found between 1475–1390 cm^{-1} with strong vibration [53] within the binder [91]. Kiefer et al. [19] also assigned C–O (CO_3^{2-}) bond asymmetric stretching vibration to wavenumber 1421–1458 cm^{-1}. Yu et al. [27] observed CO_3^{2-} asymmetrical stretching frequency around 1410 cm^{-1}, while El-Didamony et al. [80] claimed that the interaction of atmospheric CO_2 with the hydroxyl of cations caused the formation of calcite, as shown in Equation (8).

$$CO_2 + Ca(OH)_2 \rightarrow CaCO_3 + H_2O \quad (8)$$

Furthermore, the carbonate band has been reported to be more pronounced in OPC and AAB spectra compared to GP products, as shown in Figure 5. Jang et al. [93] reported that GP binder exposure to CO_2 causes an increase in the Si/Al ratio due to silicate unit alteration by the infusion of CO_2 from the atmosphere compared to what is obtainable in the seal-up samples. They also noticed that the incorporation of MgO into a GP product could reduce CO_2 diffusivity thereby increasing the compressive strength of the binder. The atmospheric CO_2 has been reported to have a stretching band at 2350 cm^{-1} and bending at 660 cm^{-1} [92,94]. Hence, FTIR spectra can be used to monitor the level of carbonation of aluminosilicate and OPC binders. Carbonate stretching vibration occurred at 1390–1420 cm^{-1}, while CO_3^{2-} from $CaCO_3$ was noted to vibrate around 871- 874 cm^{-1} and 1792–2516 cm^{-1}.

2.4. FTIR Spectra Vibrations for Ca(OH)$_2$, -OH, H-OH, and Si-OH

Stolper [54] posits that the H-O-H and Si-OH/H-OH ratios influence the equilibrium constant between Si-OH bonds and hydrogen bonds. How hydrogen bonds influence the absorption of IR light depends on the amount of each reactant used in the synthesis. This suggests that an increase in -OH- production from the alkaline activator (Na/KOH_{aq}) or precipitated Portlandite ($Ca(OH)_2$) could lead to an increase in the intensity of -OH and Si-OH groups vibrating at 3500–3600 cm^{-1}. Bands of vibration between 2750 and 2800 cm^{-1} are associated with the asymmetric stretching of H-O-H formed by hydrogen bonding, whereas the bending vibration is associated with 1623–1650 cm^{-1}, according to other researchers [63,71].

Due to the formation of hydrogen bonding from thaumasite interaction (CaSi-OH), this bond is also observed in the IR spectra of the sulfate attack of Na_2SO_4 [65], but not on $MgSO_4$ salt. The formation of hydrogen bonds could reduce the frequency of Si-OH bonds. Thus, there was structural retention of hydroxyl bonds in the $MgSO_4$-exposed sample [66]. Due to Si-O-H stretching or OH bending, the spectra of low and high NaOH concentrations are distinguished by a shoulder peak at 875 cm^{-1} [95]. As noted by Atta et al. [32], the disappearance of H-O-H bending (1789 cm^{-1}) was due to the reactivity of acidic silanol (Si-OH) with alkali. Hydrogen-bound hydroxyl (H-OH) was assigned the frequency of 3424 cm^{-1}, while intermolecular water was assigned the frequency of 3124 cm^{-1}. Consequently, FTIR could be used to qualitatively distinguish between the concentration of hydroxyl ions and the pH of cementitious binder products.

3. The Use of FTIR Spectra for Binder Durability

FTIR can be used to determine the extent of sulfate or acidic attack qualitatively, as reported by other researchers [86,96–99], by specifically studying the spectra bands—H-O-H and OH^-.

3.1. The Effect of an Acidic Attack on the H-O-H and S-O-T Bond Vibrations in FTIR Spectra

When a cementitious binder is exposed to acetic and sulfuric acids, the intensity and frequency of the H-O-H and $Ca(OH)_2$ vibration bands may increase [100–103]. Garcia-Lodeiro et al. [45,67,74,99,104] and Yu et al. [27] attributed the range 3500–3640 cm^{-1} to OH^- (Portlandite), while asymmetric stretching (3437–3441 cm^{-1}) and bending of H-O-H molecules (1637 cm^{-1}) were also reported. Another significant band is the bending vibration of unbound water molecules at 1500–1700 cm^{-1}, while the band at 1635 cm^{-1}

is for adsorbed water molecules within the silica formation. The stability of hydrogen bonding also depends on the basicity of the electron's donor site, which increases down the group in the periodic table of elements [105]. Garcia-Lodeiro et al. [45,74] observed the disappearance of the hydroxyl (OH) band due to an acidic attack at 3500 cm^{-1} due to hydroxonium formation and ion exchanges [106–109].

Furthermore, Korolevich et al. [110] observed the bending vibration of hydroxyl due to the formation of hydrogen bonding H-O-H at 1613–1667 cm^{-1}. Geng et al. [111] observed water within the microstructures of jennite and tobermorite-like C-S-H systems of short-order length chain (Q^1 and Q^2). It is important to state that the presence of excessive -OH groups diminish the compressive strength of the binder. Yusuf et al. [100] showed that FTIR spectra (Figure 12) reflected cation detachment from C-S-H or C-(A)-S-H by sulfuric acid attack. Detachment of Ca^{2+} from CASH led to an increase in the frequency of vibration of Si-O-T from 1021 cm^{-1} to 1097 cm^{-1}. This caused an increment in the wavenumber of Si-O-T vibration. This also reflects in the bending vibration of Si-O-T at the wavenumber 463 cm^{-1} in comparison with an acid-attacked sample at 449 cm^{-1} due to decalcification. The same observation was reported by Bakharev et al. [103], showing that concentration could also influence the shift in the band of Si-O-T.

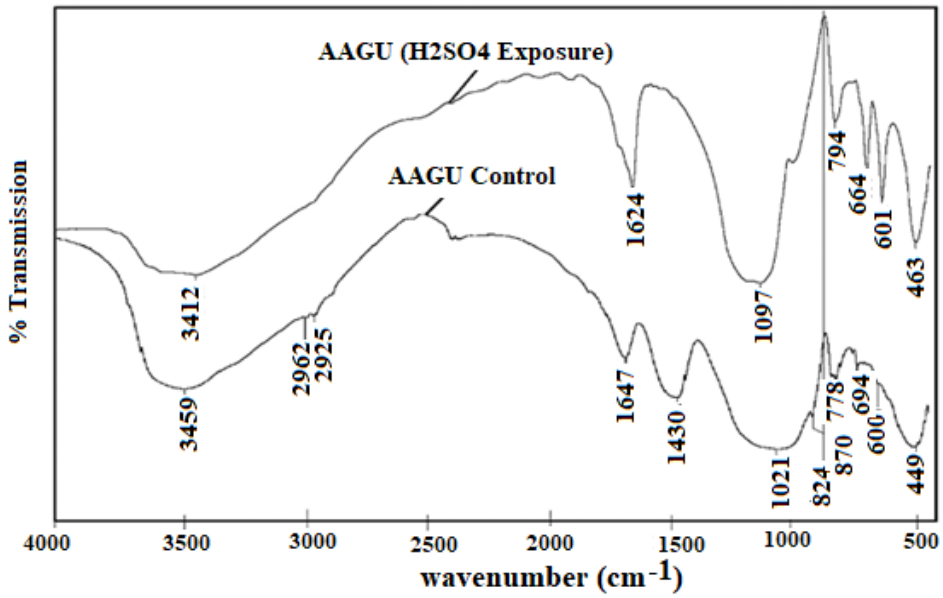


Figure 12. Sulfuric acid attack of palm oil fuel ash/slag alkaline binders (From JMCE Ref. [100] and used with permission).

3.2. The Effect of a Sulfate Attack on the H-O-H Bond and Si-O-T Vibrations in FTIR Spectra

The type of cation in the binder is a significant factor that can affect the position of the band. On this note, Ismail et al. [66] exposed a fly ash GP sample to $MgSO_4$ and Na_2SO_4 solutions, and Yusuf et al. [28] exposed an alkaline-activated palm oil fuel ash/slag to the same solution. FTIR spectra have shown a different pattern of spectra due to sulfate exposures in GP [66] and AAB [28] systems with lower and higher Si/Al ratios in the precursors used for the synthesis, respectively. Regardless of the binder types, FTIR observed the same characteristics when H-O-H/OH and S-O-T were observed in both systems (Figures 13 and 14) with reference to the control samples. It was reported that exposing the samples to a sulfate attack could cause ion exchange due to decalcification in AAB systems and the dealumination in GP systems. The skeletal frameworks were dominated by CASH and NASH, respectively.

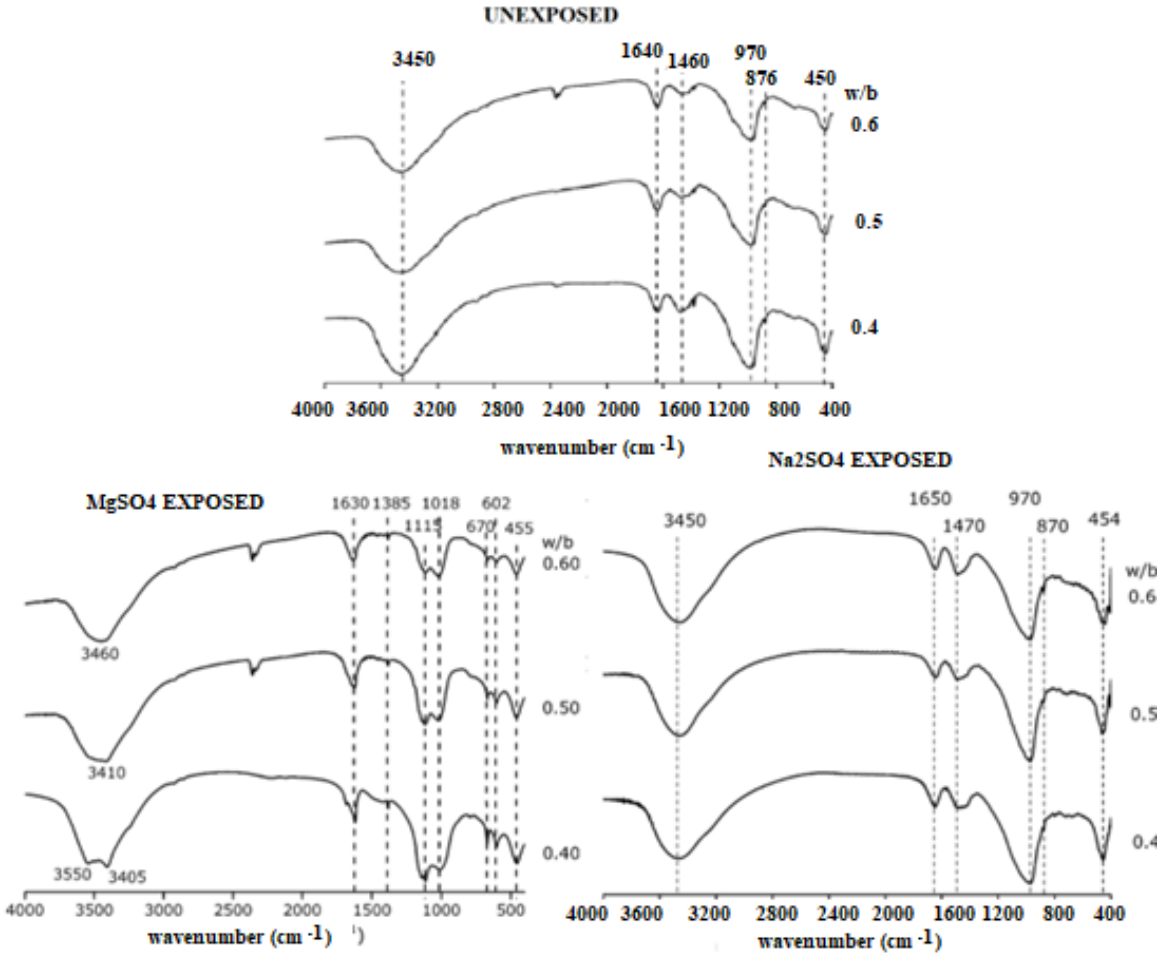


Figure 13. Effect of a sulfate attack on a Si-O-T band (From RILEM Ref. [66] and used with permission).

The spectra band (Si-O-T) of the samples and the control (Figure 13) were observed and it was discovered that ion exchanges occurred. The presence of gypsum led to the vibration of S-O bonds at 602 and 670 cm^{-1} in the $MgSO_4$-exposed fly ash/slag geopolymer, but it was absent in Na_2SO_4 exposure. However, in the AAB system, there was a remarkable shift in S-O bands from 690 to 691 cm^{-1} in $MgSO_4$ and Na_2SO_4, respectively (Figure 14). This indicates the disintegration and depolymerization of Si-O-Si(Al) due to the removal of Al^{3+} and Ca^{2+} in GP and AAB systems, respectively, to form gypsum ($CaSO_4$). Fernandez-Carrasco [23] found sulfate (S-O) vibrations from a gypsum or sulfate attack with their water of crystallization at 658–668 cm^{-1} (triplet band).

In Figure 13, the asymmetric stretching of the Si-O-Si(Al) band at 970 cm^{-1} in the control shifted to 1018 and 1115 cm^{-1}, and its bending vibration shifted from 450 cm^{-1} to 454 and 455 cm^{-1}, respectively, in Na and Mg sulfates, respectively, due to dealumination. A similar effect was observed in the AAB system (Figure 14) [28] due to decalcification at 1021 cm^{-1} in the control became 1027 and 1033 cm^{-1} in Mg sulfate and Na sulfate, respectively. Similarly, the Si-O-T bending vibration increased from 449 to 457 and 459 cm^{-1}, respectively.

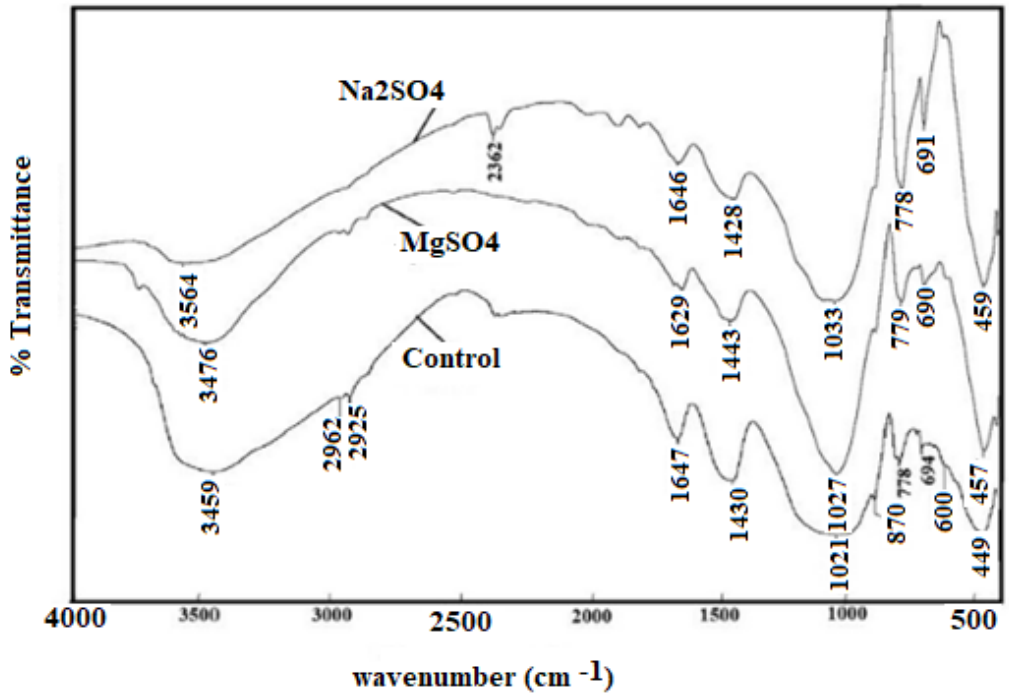


Figure 14. The effect of a sulfate attack on a Si-O-T band (From Elsevier Ref. [28] and used with permission).

The water/cement (w/c) ratio in the binder could also affect the crystallization of the sample (Figure 13). Sulfate has a greater impact on the binder because a higher water/binder ratio promotes crystallization and the proliferation of hydroxyl ions due to hydrogen bonding. In the GP system, the $MgSO_4$-exposed sample prepared at w/b = 0.6 had greater HOH/OH vibration (3460 cm^{-1}) than the control (3450 cm^{-1}) and became 3410 cm^{-1} at a lower w/b ratio = 0.5, but no changes were observed in the spectra of Na_2SO_4-exposed regardless of w/b ratios [70]. The $MgSO_4$-exposed sample had more C-O vibration (CO_2) vibrating at 2350 cm^{-1}, indicating a higher w/b ratio of 0.5 and 0.6, but this was not present in the Na_2SO_4-exposed sample (SES). The C-O vibration caused by calcite (CO_3^{2-}) is more pronounced in the SES, but it is absent in the $MgSO_4$-exposed sample (MES) [94,96].

In the AAB system (Figure 14), the SES has more C-O stretching vibration (CO_2) at 2362 cm^{-1}, while the C-O from CO_3^{2-} vibrated at a lower frequency of 1428 cm^{-1} in the SES compared to the MES (1443 cm^{-1}) and the control sample (1430 cm^{-1}). As a result of the presence of alkali present in the activator, calcite formation is more likely in the SES or MES, according to Equation (9) [5].

$$2NaOH + CO_2 \rightarrow Na_2CO_3 + H_2O \quad (9)$$

Furthermore, as shown in Figure 14, the frequency of vibration of H-O-H and OH bonds in Na_2SO_4 (3564 cm^{-1}) and $MgSO_4$ (3476 cm^{-1}) was higher than in the control sample (3459 cm^{-1}). This could be due to the formation of additional water, as shown in Equation (9). Bakharev [86] also established that an increase in vibration by molecular water at 1600 cm^{-1} could be due to a sulfate attack, as was clearly observed through H-O-H vibration bands, as shown in Figure 15. A sulfate attack reduces the molecular water vibration bands, as shown in Figs. 13 and 14, in the $MgSO_4$-exposed GP (1640 to 1630 cm^{-1}) and AAB (1647 to 1629 cm^{-1}) [28].

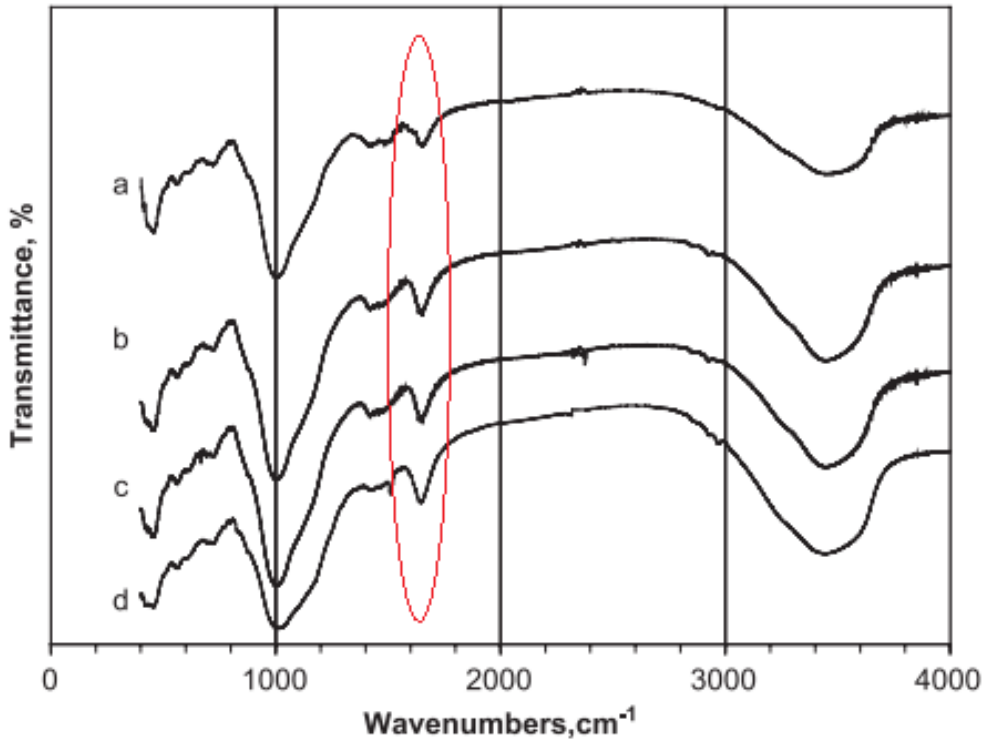


Figure 15. Variation in the vibration of molecular water due to a sulfate attack (a) control, (b) 5% sodium sulfate exposure, (c) 5% magnesium sulfate exposure, and (d) combination (From Elsevier Ref. [86] and used with permission).

Therefore, the destruction of OPC or GP binders by acid or a sulfate attack is caused by the destruction of the Si-O-T structural framework as a result of the removal of calcium and the formation of sulfate-based expansive structures, such as ettringite and gypsum. Due to the reaction of Portlandite with sulfate compounds, OPC will sustain more damage than GP or AAB. Finally, Table 1 shows the summary of the major bands essential to the characterization of cementitious binders by using the FTIR technique.

Table 1. Some of the significant bands in the FTIR spectra of cementitious materials.

Bonds	Wavenumber	Assignment	References
Si-O-T	950–1200 cm^{-1}	Very strong band of asymmetric stretching	[22,23,63,65,112,113]
Si-O-T	1116–1148 cm^{-1}	Unreacted sample of metakaolin and rice husk ash	[32,113,114]
Si-O-T	671–717 cm^{-1}	symmetric stretching of Si-O-T	[60,63,80]
Si-O-T	435–540 cm^{-1}	Bending	[22,23,63,65,77]
-Si-OH	815–988 cm^{-1} (Q^2Al)	Symmetric stretching	[63,69]
-C-O	1421–1458 cm^{-1}	Very strong stretching vibration (CO_3^{2-})	[14,24,27,44,69,113,115,116]
-C-O	2350-2355 cm^{-1}	Asymmetric stretching (CO_2)	[94–96]
-C-O	875–877 cm^{-1}	Strong vibration (CO_2)	[10,95,113]
S-O (SO_4)	1115–1200 cm^{-1}	Very strong sulfate asymmetrical vibration	[10,14,23]
S-O (SO4)	660–667 cm^{-1}	Bending vibration strong in $CaSO_4$ and weak in Na_2SO_4	[13,61,66,95]

Table 1. *Cont.*

Bonds	Wavenumber	Assignment	References
-N-O (NO_3)	1385 cm^{-1}	Very strong diffuse asymmetric stretching	[3,10]
-N-O (NO_3)	815–840 cm^{-1}	Symmetric stretching of nitrate	[10,95]
-P-O (PO_4)	1000–1100 cm^{-1}	Asymmetric stretching	[10,95]
Si-O-Si	795 cm^{-1}	Symmetric stretching	[3,116]
Si-O-Si, O-Si-O	470 cm^{-1}	bending	[22,23,33,63,65,67,113,117]
Si-O	1010–1104 cm^{-1}	Kaolinite in-plane vibration	[117]
T-O	452 cm^{-1}	Associated with the T-O bending	[32]
kaolinite	435 cm^{-1}	Strong kaolinite bending	[33,117]
Al-O	600–800 cm^{-1}	Alumina in IV-fold coordination	[87,118]
-OH/HOH	3500–3600 cm^{-1}	-asymmetric stretching	[33,117,119]
-OH	875 cm^{-1}	bending	[33,117,119]
Al-O	700 cm^{-1}	Tetrahedra alumina	[120]
Al-O	620 cm^{-1}	Octahedral alumina	[120]
Si-OH	875 cm^{-1}	Stretching bank	[117]
H-O-H	2350–2800 cm^{-1}	-asymmetric stretching	[14,33,117,121]
H-O-H	2810–2924.5 cm^{-1}	Hydrogen bonding	[10,121]
H-O-H	1500–1700 cm^{-1}	Unbound water molecules	[122]
H-O-H	1622–1652 cm^{-1}	Bending vibration	[75,76,113]

4. Conclusions

Fourier-transform infrared (FTIR) spectroscopy is a very useful tool for the characterization of bonds that exist within the products of cementitious binders, such as calcium silicate hydrate (C-S-H) in ordinary Portland cement (OPC), calcium aluminosilicate (C-A-S-H) in alkaline-activated binders (AABs) or slag (AAS), and sodium/potassium aluminosilicate (Na/K-A-S-H) bonds in geopolymers (GPs). The prominent bands include Si-O, Si-O-T, Si-OH, -OH, HOH, C-O (CO_3^{2-}), and S-O, which can be found in 600–800 cm^{-1}, 950–1055 cm^{-1}, 800–890 cm^{-1}, 3400–3465 cm^{-1}, 1390–1450 cm^{-1}, and 602–670 cm^{-1}, respectively. The bending vibration of Si-O-T may also be found within the wavenumber range of 400–600 cm^{-1}. Other conclusions include the following:

(a) FTIR is a simple technique for bond characterization and its sampling methods include transmission, attenuated total reflectance (ATR), diffusive reflectance infrared transmittance spectroscopy technique (DRIFTS), and specular aperture grazing angle (SAGA).
(b) FTIR can be used to study the aluminosilicate and calcium silicate hydrate bond characteristics in the cementitious binders which include traditional cement (OPC), geopolymers (GPs), and alkaline-activated slag or binders (AASs). The attachment of cations and their atomic weight have effects on the skeletal framework and the frequency of vibration of Si-O-T bonds.
(c) FTIR could give an indication of the crystalline nature of the binder, thereby giving hints on the silicate organization by observing Si-O-T within 900–1100 cm^{-1}. The more the frequency of vibration of the Si-O-Si bond, the more the silicate re-organizes or polymerizes the binder.
(d) FTIR spectra bands could also be used to study the durability of a binder qualitatively by observing the Si-O-T and -OH bands upon being exposed to aggressive environments, such as sulfates and acids.

Funding: The author extends his appreciation to the Deanship for Research and Innovation Ministry of Education in Saudi Arabia for funding this research through project No. IFP-A-2022-1-10.

Institutional Review Board Statement: Not applicable.

Informed Consent Statement: Not applicable.

Data Availability Statement: Not applicable.

Acknowledgments: The author would like to appreciate the remarks of the anonymous reviewer which have greatly improved the manuscript. The continuous support of the University of Hafr Al Batin is appreciated.

Conflicts of Interest: The author declares no conflict of interest.

References

1. Kristó, J.; Frost, R.; Felinger, A.; Mink, J. FTIR spectroscopic study of intercalated kaolinite. *J. Mol. Struct.* **1997**, *410–411*, 119–122. [CrossRef]
2. Ketov, A.; Rudakova, L.; Vaisman, I.; Ketov, I.; Haritonovs, V.; Sahmenko, G. Recycling of rice husks ash for the preparation of resistant, lightweight and environment-friendly fired bricks. *Constr. Build. Mater.* **2021**, *302*, 124385. [CrossRef]
3. Lee, W.K.W.; van Deventer, J.S.J. The Effect of Inorganic Salt contamination on the strength and durability of geopolymers. *Colloids Surf. A Physicochem. Eng. Asp.* **2002**, *211*, 115–126. [CrossRef]
4. van Jaarsveld, J.; van Deventer, J. The effect of metal contaminants on the formation and properties of waste-based geopolymers. *Cem. Concr. Res.* **1999**, *29*, 1189–1200. [CrossRef]
5. Davidovits, J. Application of Ca-based geopolymer with blast furnace slag, a review. In Proceedings of the Second International Slag Valorisation Symposium, Leuven, Belgium, 18–20 April 2011; pp. 33–49.
6. Davidovits, J. *Geopolymer Chemistry and Applications*; Geopolymer Institute: Saint-Quentin, France, 2008.
7. Van Jaarsveld, J.; van Deventer, J.; Lukey, G. The characterization of source materials in fly ash-based geopolymers. *Mater. Lett.* **2003**, *57*, 1272–1280. [CrossRef]
8. King, P.L.; Mcmillan, P.F.; Moore, G.M. *Infrared Spectroscopy of Silicate Glasses with Application to Natural Systems*; Mineralogical Association of Canada: Ottawa, ON, Canada, 2004.
9. Fadlelmoula, A.; Pinho, D.; Carvalho, V.H.; Catarino, S.O.; Minas, G. Fourier Transform Infrared (FTIR) Spectroscopy to Analyse Human Blood over the Last 20 Years: A Review towards Lab-on-a-Chip Devices. *Micromachines* **2022**, *13*, 187. [CrossRef]
10. Coates, J. *Encyclopedia of Analytical Chemistry*; Meyers, R.A., Ed.; John Wiley & Sons Ltd.: Chichester, UK, 2000; pp. 10815–10837.
11. Dumas, P.; Sockalingum, G.D.; Sulé-Suso, J. Adding synchrotron radiation to infrared microspectroscopy: What's new in biomedical applications? *Trends Biotechnol.* **2007**, *25*, 40–44. [CrossRef]
12. Kylili, A.; Fokaides, P.A.; Christou, P.; Kalogirou, S.A. Infrared thermography (IRT) applications for building diagnostics: A review. *Appl. Energy* **2014**, *134*, 531–549. [CrossRef]
13. Hermann, P.; Kästner, B.; Hoehl, A.; Kashcheyevs, V.; Patoka, P.; Ulrich, G.; Feikes, J.; Ries, M.; Tydecks, T.; Beckhoff, B.; et al. Enhancing the sensitivity of nano-FTIR spectroscopy. *Opt. Express* **2017**, *25*, 16574–16588. [CrossRef]
14. Kiefer, J.; Stärk, A.; Kiefer, A.L.; Glade, H. Infrared Spectroscopic Analysis of the Inorganic Deposits from Water in Domestic and Technical Heat Exchangers. *Energies* **2018**, *11*, 798. [CrossRef]
15. Keller, W.D.; Spotts, J.H.; Biggs, D.L. Infrared Spectra of some rock forming materials. *Am. J. Sci.* **1952**, *250*, 438–471. [CrossRef]
16. De Lloyd, D. Instrumental Infrared and Fourier Transform Spectroscopy. Delloyd's Lab Tech Resources, Reagents and Instrumentation. 2000. Available online: http://delloyd.50megs.com/MOBILE/infrared_spectroscopy.html (accessed on 18 February 2023).
17. Filip, Z.; Hermann, S.; Demnerová, K. FT-IR spectroscopic characteristics of differently cultivated Escherichia coli. *Czech J. Food Sci.* **2008**, *26*, 458–463. [CrossRef]
18. Mylläri, V.; Ruoko, T.-P.; Syrjälä, S. A comparison of rheology and FTIR in the study of polypropylene and polystyrene photodegradation. *J. Appl. Polym. Sci.* **2015**, *132*. [CrossRef]
19. Sagar, A. Infrared (IR) Spectroscopy-Definition, Principle, Parts, Uses. 2022. Available online: https://microbenotes.com/infrared-ir-spectroscopy/ (accessed on 25 December 2022).
20. Cooley, J.W.; Tukey, J.W. An Algorithm for the Machine Calculation of Complex Fourier Series. *Math. Comput.* **1965**, *19*, 297–301. [CrossRef]
21. Daudon, M.; Bazin, D. Vibrational spectroscopies to investigate concretions and ectopic calcifications for medical diagnosis. *Comptes Rendus Chim.* **2016**, *19*, 1416–1423. [CrossRef]
22. Afremow, L.C.; Vanderberg, J.T. High resolution spectra of inorganic pigments and extenders in the mid-infrared region from 1500 cm^{-1} to 200 cm^{-1}. *J. Paint Technol.* **1966**, *38*, 169–202.
23. Fernández-Carrasco, L.; Torrens-Martín, D.; Morales, L.M.; Martínez-Ramírez, S. Infrared Spectroscopy in the Analysis of Building and Construction Materials. In *Infrared Spectroscopy—Materials Science, Engineering and Technology*; IntechOpen: London, UK, 2012. [CrossRef]

24. Beasley, M.M.; Bartelink, E.J.; Taylor, L.; Miller, R.M. Comparison of transmission FTIR, ATR, and DRIFT spectra: Implications for assessment of bone bioapatite diagenesis. *J. Archaeol. Sci.* **2014**, *46*, 16–22. [CrossRef]
25. Davidovits, J. *Properties of Geopolymer Cement*; Geopolymer Institute: Saint-Quentin, France, 1994; pp. 1–19.
26. Brown, T.L. Infrared Intensities And Molecular Structure. *Chem. Rev.* **1958**, *58*, 581–608. [CrossRef]
27. Yu, P.; Kirkpatrick, R.J.; Poe, B.; McMillan, P.F.; Cong, X. Structure of Calcium Silicate Hydrate (C-S-H): Near-, Mid-, and Far-Infrared Spectroscopy. *J. Am. Ceram. Soc.* **2004**, *82*, 742–748. [CrossRef]
28. Yusuf, M.O. Performance of slag blended alkaline activated palm oil fuel ash mortar in sulfate environments. *Constr. Build. Mater.* **2015**, *98*, 417–424. [CrossRef]
29. Yusuf, M.O.; Johari, M.A.M.; Ahmad, Z.A.; Maslehuddin, M. Impacts of silica modulus on the early strength of alkaline activated ground slag/ultrafine palm oil fuel ash based concrete. *Mater. Struct.* **2014**, *48*, 733–741. [CrossRef]
30. Yusuf, M.O.; Johari, M.A.M.; Ahmad, Z.A.; Maslehuddin, M. Effects of addition of Al(OH)3 on the strength of alkaline activated ground blast furnace slag-ultrafine palm oil fuel ash (AAGU) based binder. *Constr. Build. Mater.* **2014**, *50*, 361–367. [CrossRef]
31. Yusuf, M.O.; Johari, M.A.M.; Ahmad, Z.A.; Maslehuddin, M. Evolution of alkaline activated ground blast furnace slag–ultrafine palm oil fuel ash based concrete. *Mater. Des.* **2014**, *55*, 387–393. [CrossRef]
32. Atta, A.; Jibril, B.; Aderemi, B.; Adefila, S. Preparation of analcime from local kaolin and rice husk ash. *Appl. Clay Sci.* **2012**, *61*, 8–13. [CrossRef]
33. Uchino, T.; Sakka, T.; Hotta, K.; Iwasaki, M.; Uchino, T.; Sakka, T.; Hotta, K.; Iwasaki, M. Attenuated Toatal Reflectance Fourier-Transform Infrared Spectra of a Hydrated Sodium Soilicate Glass. *J. Am. Ceram. Soc.* **1989**, *72*, 2173–2175. [CrossRef]
34. Setnička, V. FT-IR Reflection Techniques. 2021. Available online: https://old.vscht.cz/anl/vibspec/FTIR%20Reflection%20Techniques.pdf (accessed on 25 December 2022).
35. ASTM C494/C494M-08. Standard Specification for Chemical Admixtures for Concrete. 2008. Available online: https://webstore.ansi.org/standards/astm/astmc494c494m08a (accessed on 31 December 2022).
36. Rees, C.A.; Provis, J.L.; Lukey, G.C.; van Deventer, J.S.J. Attenuated Total Reflectance Fourier Transform Infrared Analysis of Fly Ash Geopolymer Gel Aging. *Langmuir* **2007**, *23*, 8170–8179. [CrossRef]
37. Nedeljković, M.; Šavija, B.; Zuo, Y.; Luković, M.; Ye, G. Effect of natural carbonation on the pore structure and elastic modulus of the alkali-activated fly ash and slag pastes. *Constr. Build. Mater.* **2018**, *161*, 687–704. [CrossRef]
38. Michael, R.B. Infrared Spectra of Adsorbed Molecules. *Appl. Spectrosc. Rev.* **1968**, *1*, 289–378. [CrossRef]
39. Casale, A.J.; Doukakis, J.; Najm, H.; Davis, K. Quantitative Assessment of Infrared Analysis of Concrete Admixtures. *Int. J. Concr. Struct. Mater.* **2013**, *7*, 203–214. [CrossRef]
40. Fuller, M.P.; Griffiths, P.R. Diffuse reflectance measurements by infrared Fourier transform spectrometry. *Anal. Chem.* **1978**, *50*, 1906–1910. [CrossRef]
41. ThermoFisher Scientific. Effect of Water on Infrared Signal. 2023. Available online: https://www.thermofisher.com/blog/identifying-threats/how-water-affects-raman-and-ftir-identification-of-unknown-substances/#:~:text=FTIR%20is%20often%20blinded%20or,overwhelming%20signal%20produced%20by%20water (accessed on 25 December 2022).
42. Zhang, X.; He, A.; Guo, R.; Zhao, Y.; Yang, L.; Morita, S.; Xu, Y.; Noda, I.; Ozaki, Y. A new approach to removing interference of moisture from FTIR spectrum. *Spectrochim. Acta Part A: Mol. Biomol. Spectrosc.* **2021**, *265*, 120373. [CrossRef]
43. Giordanengo, T.; Charpentier, J.-P.; Roger, J.-M.; Roussel, S.; Brancheriau, L.; Chaix, G.; Baillères, H. Correction of moisture effects on near infrared calibration for the analysis of phenol content in eucalyptus wood extracts. *Ann. For. Sci.* **2008**, *65*, 803. [CrossRef]
44. Povnnennykh, A.S. The use of infrared spectra for the determination of minerals. *Am. Mineral.* **1978**, *63*, 956–959.
45. Lodeiro, I.G.; Fernández-Jimenez, A.; Palomo, A.; Macphee, D. Effect on fresh C-S-H gels of the simultaneous addition of alkali and aluminium. *Cem. Concr. Res.* **2010**, *40*, 27–32. [CrossRef]
46. Provis, J.L. Geopolymers and other alkali activated materials: Why, how, and what? *Mater. Struct.* **2014**, *47*, 11–25. [CrossRef]
47. Fernández-Jiménez, A.; Palomo, A. Composition and microstructure of alkali activated fly ash binder: Effect of the activator. *Cem. Concr. Res.* **2005**, *35*, 1984–1992. [CrossRef]
48. Hunt, J.M.; Wisherd, M.P.; Bonham, L.C. Infrared Absorption Spectra of Minerals and Other Inorganic Compounds. *Anal. Chem.* **1950**, *22*, 1478–1497. [CrossRef]
49. Farmer, V. *The Infrared Spectra of Minerals*; Mineralogical Society of Great Britain and Ireland: Twickenham, UK, 1974. [CrossRef]
50. Nakamoto, K. Infrared Spectra of Inorganic and Coordination Compounds. In *Handbook of Vibrational Spectroscopy*; Griffiths, P.R., Ed.; Wiley: New York, NY, USA, 1970. [CrossRef]
51. Bensted, J. Uses of Raman Spectroscopy in Cement Chemistry. *J. Am. Ceram. Soc.* **1976**, *59*, 140–143. [CrossRef]
52. Bensted, J.; Varma, S.P. *Some Applications in Infrared and Raman Spectral Studies in Cement Industry (Part 2: Portland Cement and Its Constituents)*; Cement Technology: Covington, GA, USA, 1974; pp. 378–382.
53. Ghosh, S.N.; Handoo, S.K. Infrared and Raman spectral studies in cement and concrete (review). *Cem. Concr. Res.* **1980**, *10*, 771–782. [CrossRef]
54. EStolper, E. Contributions to Mineralogy and Petrology Water in Silicate Glasses: An Infrared Spectroscopic Study. *Contrib. Mineral. Petrol.* **1982**, *81*, 1–17. [CrossRef]
55. Wallah, S.E.; Rangan, B.V. *Low-Calcium Fly Ash-Based Geopolymer Concrete: Long-Term Properties*; Curtin University of Technology: Perth, Australia, 2006; p. 107. [CrossRef]

56. Lloyd, N.A.; Rangan, B.V. Geopolymer concrete with fly ash. In Proceedings of the Second International Conference on Sustainable Construction Materials and Technologies, Ancona, Italy, 28–30 June 2010; Volume 3, pp. 1493–1504.
57. Bartholomew, R.F.; Butler, B.L.; Hoover, H.L.; Wu, C.K. Infrared Spectra of a Water-Containing Glass. *J. Am. Ceram. Soc.* **1980**, *63*, 481–485. [CrossRef]
58. Williams, G.P. The national synchrotron light source in the infrared region. *Nucl. Instruments Methods Phys. Res.* **1982**, *195*, 383–387. [CrossRef]
59. Mawhinney, D.B.; Glass, J.J.A.; Yates, J.J.T. FTIR Study of the Oxidation of Porous Silicon. *J. Phys. Chem. B* **1997**, *101*, 1202–1206. [CrossRef]
60. Karakassides, M.A. An Infrared Reflectance Study of Si-O Vibrations in Thermally Treated Alkali-Saturated Montmorillonites. *Clay Miner.* **1999**, *34*, 429–438. [CrossRef]
61. Tararushkin, E.V.; Shchelokova, T.N.; Kudryavtseva, V.D. A study of strength fluctuations of Portland cement by FTIR spectroscopy. *IOP Conf. Series: Mater. Sci. Eng.* **2020**, *919*. [CrossRef]
62. Criado, M.; Palomo, A.; Fernandezjimenez, A. Alkali activation of fly ashes. Part 1: Effect of curing conditions on the carbonation of the reaction products. *Fuel* **2005**, *84*, 2048–2054. [CrossRef]
63. Lecomte, I.; Henrist, C.; Liégeois, M.; Maseri, F.; Rulmont, A.; Cloots, R. (Micro)-structural comparison between geopolymers, alkali-activated slag cement and Portland cement. *J. Eur. Ceram. Soc.* **2006**, *26*, 3789–3797. [CrossRef]
64. Provis, J.; van Deventer, J. What controls the durability of geopolymer binders and concretes. In *Concrete under Severe Conditions, Two Volume Set*; CRC Press: Boca Raton, FL, USA, 2010; pp. 1535–1542. [CrossRef]
65. Lodeiro, I.G.; Macphee, D.; Palomo, A.; Fernández-Jiménez, A. Effect of alkalis on fresh C–S–H gels. FTIR analysis. *Cem. Concr. Res.* **2009**, *39*, 147–153. [CrossRef]
66. Ismail, I.; A Bernal, S.; Provis, J.L.; Hamdan, S.; Van Deventer, J.S.J. Microstructural changes in alkali activated fly ash/slag geopolymers with sulfate exposure. *Mater. Struct.* **2012**, *46*, 361–373. [CrossRef]
67. García-Lodeiro, I.; Jimenez, A.M.F.; Blanco-Varela, M.T.; Palomo, A. FTIR study of the sol–gel synthesis of cementitious gels: C–S–H and N–A–S–H. *J. Sol-Gel Sci. Technol.* **2007**, *45*, 63–72. [CrossRef]
68. Hubicki, Z.; Zieba, E.; Wójcik, G.; Ryczkowski, J. FT-IR/PAS and SEM EDX Studies on Aluminosilicates Modified by Cs(I), Th(IV) and U(VI). *Acta Phys. Pol. A* **2009**, *116*, 312–314. [CrossRef]
69. García-Lodeiro, I.; Maltseva, O.; Fernández-Jiménez, A.; Torroja, I.E. Hybrid alkaline cement: Part I Fundamentals. *Rev. Română Mater./Rom. J. Mater.* **2012**, *42*, 330–335.
70. Peyvandi, A.; Holmes, D.; Soroushian, P.; Balachandra, A.M. Monitoring of Sulfate Attack in Concrete by Al27 and Si29 MAS NMR Spectroscopy. *J. Mater. Civ. Eng.* **2015**, *27*. [CrossRef]
71. Kramar, S.; Ducman, V. Mechanical and microstructural characterization of geopolymer synthesized from low calcium fly ash. *Chem. Ind. Chem. Eng. Q.* **2015**, *21*, 13–22. [CrossRef]
72. Xu, Z.; Cornilsen, B.C.; Popko, D.C.; Wood, J.R.; Hwang, J.-Y. Quantitative Mineral Analysis by FTIR Spectroscopy. *Internet J. Vib. Spectrosc.* **2001**, *5*, 4.
73. Chen, J.J.; Thomas, J.J.; Taylor, H.F.; Jennings, H.M. Solubility and structure of calcium silicate hydrate. *Cem. Concr. Res.* **2004**, *34*, 1499–1519. [CrossRef]
74. García-Lodeiro, I.; Jimenez, A.M.F.; Palomo, A.; Macphee, D. Effect of Calcium Additions on N-A-S-H Cementitious Gels. *J. Am. Ceram. Soc.* **2010**, *93*, 1934–1940. [CrossRef]
75. Rovnaník, P. Influence of C12A7 admixture on setting properties of fly ash geopolymer. *Ceramics—Silikaty* **2010**, *54*, 362–367.
76. Rovnaník, P. Effect of curing temperature on the development of hard structure of metakaolin-based geopolymer. *Constr. Build. Mater.* **2010**, *24*, 1176–1183. [CrossRef]
77. Gougazeh, M.; Buhl, J.-C. Synthesis and characterization of zeolite A by hydrothermal transformation of natural Jordanian kaolin. *J. Assoc. Arab. Univ. Basic Appl. Sci.* **2014**, *15*, 35–42. [CrossRef]
78. Lloyd, N.A.; Rangan, B.V. Geopolymer Concrete: A Review of Development and Opportunities. In Proceedings of the 35th Conference on Our World in Concrete and Structure, Singapore, 25–27 August 2010.
79. Criado, M.; Fernández-Jiménez, A.; de la Torre, A.G.; Aranda, M.A.G.; Palomo, A. An XRD study of the effect of the SiO2/Na2O ratio on the alkali activation of fly ash. *Cem. Concr. Res.* **2007**, *37*, 671–679. [CrossRef]
80. El-Didamony, H.; Amer, A.A.; Ela-Ziz, H.A. Properties and durability of alkali-activated slag pastes immersed in sea water. *Ceram. Int.* **2012**, *38*, 3773–3780. [CrossRef]
81. Criado, M.; Aperador, W.; Sobrados, I. Microstructural and Mechanical Properties of Alkali Activated Colombian Raw Materials. *Materials* **2016**, *9*, 158. [CrossRef] [PubMed]
82. Yusuf, M.O.; Johari, M.A.M.; Ahmad, Z.A.; Maslehuddin, M. Influence of curing methods and concentration of NaOH on strength of the synthesized alkaline activated ground slag-ultrafine palm oil fuel ash mortar/concrete. *Constr. Build. Mater.* **2014**, *66*, 541–548. [CrossRef]
83. Yusuf, M.O.; Johari, M.A.M.; Ahmad, Z.A.; Maslehuddin, M. Effects of H2O/Na2O molar ratio on the strength of alkaline activated ground blast furnace slag-ultrafine palm oil fuel ash based concrete. *Mater. Des.* **2014**, *56*, 158–164. [CrossRef]
84. Palomo, A.; Fernández-Jiménez, A.; Criado, M. Activación alcalina de cenizas volantes. *Estudio comparativo entre activadores sódicos y potásicos.* **2006**, *56*. [CrossRef]

85. Hajimohammadi, A.; Provis, J.L.; van Deventer, J.S.J. Effect of Alumina Release Rate on the Mechanism of Geopolymer Gel Formation. *Chem. Mater.* **2010**, *22*, 5199–5208. [CrossRef]
86. Bakharev, T. Durability of geopolymer materials in sodium and magnesium sulfate solutions. *Cem. Concr. Res.* **2005**, *35*, 1233–1246. [CrossRef]
87. Clayden, N.; Esposito, S.; Aronne, A.; Pernice, P. Solid state 27Al NMR and FTIR study of lanthanum aluminosilicate glasses. *J. Non-Crystalline Solids* **1999**, *258*, 11–19. [CrossRef]
88. Taylor, H.F.W. *Cement Chemistry*, 2nd ed.; Reedwood Books: Trowbridge, UK, 1990.
89. Brindley, G.W.; McKinstry, H.A. The Kaolinite-Mullite Reaction Series: IV, The Coordination of Aluminum. *J. Am. Ceram. Soc.* **1961**, *44*, 506–507. [CrossRef]
90. Bernal, S.A.; de Gutierrez, R.M.; Provis, J.L.; Rose, V. Effect of silicate modulus and metakaolin incorporation on the carbonation of alkali silicate-activated slags. *Cem. Concr. Res.* **2010**, *40*, 898–907. [CrossRef]
91. Herting, G.; Odnevall, I. Corrosion of Aluminium and Zinc in Concrete at Simulated Conditions of the Repository of Low Active Waste in Sweden. *Corros. Mater. Degrad.* **2021**, *2*, 150–162. [CrossRef]
92. Isokoski, K.; Poteet, C.A.; Linnartz, H. Highly resolved infrared spectra of pure CO_2ice (15–75 K). *Astron. Astrophys.* **2013**, *555*, A85. [CrossRef]
93. Jang, J.; Lee, N.; Lee, H. Fresh and hardened properties of alkali-activated fly ash/slag pastes with superplasticizers. *Constr. Build. Mater.* **2014**, *50*, 169–176. [CrossRef]
94. Bekiaris, G.; Bruun, S.; Peltre, C.; Houot, S.; Jensen, L.S. FTIR–PAS: A powerful tool for characterising the chemical composition and predicting the labile C fraction of various organic waste products. *Waste Manag.* **2015**, *39*, 45–56. [CrossRef] [PubMed]
95. Miller, F.A.; Wilkins, C.H. Infrared Spectra and Characteristic Frequencies of Inorganic Ions. *Anal. Chem.* **1952**, *24*, 1253–1294. [CrossRef]
96. Elyamany, H.E.; Elmoaty, A.E.M.A.; Elshaboury, A.M. Magnesium sulfate resistance of geopolymer mortar. *Constr. Build. Mater.* **2018**, *184*, 111–127. [CrossRef]
97. Al-Akhras, N.M. Durability of metakaolin concrete to sulfate attack. *Cem. Concr. Res.* **2006**, *36*, 1727–1734. [CrossRef]
98. Karakoç, M.B.; Türkmen, I.; Maraş, M.M.; Kantarci, F.; Demirboğa, R. Sulfate resistance of ferrochrome slag based geopolymer concrete. *Ceram. Int.* **2016**, *42*, 1254–1260. [CrossRef]
99. Puertas, F.; de Gutierrez, R.; Fernández-Jiménez, A.; Delvasto, S.; Maldonado, J. Alkaline cement mortars. Chemical resistance to sulfate and seawater attack. *Mater. Constr.* **2002**, *2002*, 55–71. [CrossRef]
100. Yusuf, M.O.; Johari, M.A.M.; Ahmad, Z.A.; Maslehuddin, M. Evaluation of Slag-Blended Alkaline-Activated Palm Oil Fuel Ash Mortar Exposed to the Sulfuric Acid Environment. *J. Mater. Civ. Eng.* **2015**, *27*. [CrossRef]
101. Ariffin, M.; Bhutta, M.; Hussin, M.; Tahir, M.M.; Aziah, N. Sulfuric acid resistance of blended ash geopolymer concrete. *Constr. Build. Mater.* **2013**, *43*, 80–86. [CrossRef]
102. Bakharev, T. Resistance of geopolymer materials to acid attack. *Cem. Concr. Res.* **2005**, *35*, 658–670. [CrossRef]
103. Bakharev, T.; Sanjayan, J.; Cheng, Y.-B. Resistance of alkali-activated slag concrete to acid attack. *Cem. Concr. Res.* **2003**, *33*, 1607–1611. [CrossRef]
104. Garcia-Lodeiro, I.; Palomo, A.; Fernández-Jiménez, A.; Macphee, D. Compatibility studies between N-A-S-H and C-A-S-H gels. Study in the ternary diagram Na2O–CaO–Al2O3–SiO2–H2O. *Cem. Concr. Res.* **2011**, *41*, 923–931. [CrossRef]
105. Bakharev, T.; Sanjayan, J.G.; Cheng, Y.B. Resistance of alkali-activated slag to carbonation. *Cem. Concr. Res.* **2001**, *31*, 1277–1283. [CrossRef]
106. Nasrazadani, S.; Eghtesad, R.; Sudoi, E.; Vupputuri, S.; Ramsey, J.D.; Ley, M.T. Application of Fourier transform infrared spectroscopy to study concrete degradation induced by biogenic sulfuric acid. *Mater. Struct.* **2015**, *49*, 2025–2034. [CrossRef]
107. Satya, Y.S.D.; Saputra, E.; Olivia, M. Performance of Blended Fly Ash (FA) and Palm Oil Fuel Ash (POFA) Geopolymer Mortar in Acidic Peat Environment. *Mater. Sci. Forum* **2016**, *841*, 83–89. [CrossRef]
108. Izzat, A.M.; Mohd, A.; Al Bakri Abdullah, M.M.; Kamarudin, H. Sulfuric acid attack on ordinary Portland cement and geopolymer material. *Rev. Chim.* **2013**, *64*, 1011–1014.
109. Bhutta, M.A.R.; Ariffin, N.F.; Hussin, M.W.; Lim, N.H.A.S. Sulfate and Sulfuric Acid Resistance of Geopolymer Mortars Using Waste Blended Ash. *J. Teknol.* **2013**, *61*. [CrossRef]
110. Korolevich, M.; Zhbankov, R.; Sivchik, V. Calculation of absorption band frequencies and intensities in the IR spectrum of α-d-glucose in a cluster. *J. Mol. Struct.* **1990**, *220*, 301–313. [CrossRef]
111. Geng, G.; Taylor, R.; Bae, S.; Hernández-Cruz, D.; Kilcoyne, D.A.; Emwas, A.-H.; Monteiro, P.J. Atomic and nano-scale characterization of a 50-year-old hydrated C3S paste. *Cem. Concr. Res.* **2015**, *77*, 36–46. [CrossRef]
112. Lee, W.; van Deventer, J. The effect of ionic contaminants on the early-age properties of alkali-activated fly ash-based cements. *Cem. Concr. Res.* **2002**, *32*, 577–584. [CrossRef]
113. Panias, D.; Giannopoulou, I.P.; Perraki, T. Effect of synthesis parameters on the mechanical properties of fly ash-based geopolymers. *Colloids Surf. A Physicochem. Eng. Asp.* **2007**, *301*, 246–254. [CrossRef]
114. Sandoval, M.; Henao, J.; Ríos, C.; Williams, C.; Apperley, D. Synthesis and characterization of zeotype ANA framework by hydrothermal reaction of natural clinker. *Fuel* **2009**, *88*, 272–281. [CrossRef]
115. Barbosa, V.F.; MacKenzie, K.J.; Thaumaturgo, C. Synthesis and characterisation of materials based on inorganic polymers of alumina and silica: Sodium polysialate polymers. *Int. J. Inorg. Mater.* **2000**, *2*, 309–317. [CrossRef]

116. Mollah, M.Y.; Kesmez, M.; Cocke, D.L. An X-ray diffraction (XRD) and Fourier transform infrared spectroscopic (FT-IR) investigation of the long-term effect on the solidification/stabilization (S/S) of arsenic(V) in Portland cement type-V. *Sci. Total. Environ.* **2004**, *325*, 255–262. [CrossRef]
117. Uchino, T.; Sakka, T.; Iwasaki, M. Interpretation of Hydrated States of Sodium Silicate Glasses by Infrared and Raman Analysis. *J. Am. Ceram. Soc.* **1991**, *74*, 306–313. [CrossRef]
118. Handke, M.; Mozgawa, W. Vibrational spectroscopy of the amorphous silicates. *Vib. Spectrosc.* **1993**, *5*, 75–84. [CrossRef]
119. Stolper, E. The speciation of water in silicate melts. *Geochim. Cosmochim. Acta* **1982**, *46*, 2609–2620. [CrossRef]
120. Taylor, W.R. Application of infrared spectroscopy to studies of silicate glass structure: Examples from the melilite glasses and the systems Na2O-SiO2 and Na2O-Al2O3-SiO2. *J. Earth Syst. Sci.* **1990**, *99*, 99–117. [CrossRef]
121. Swapna, K.; Mahamuda, S.; Rao, A.S.; Shakya, S.; Sasikala, T.; Haranath, D.; Prakash, G.V. Optical studies of Sm3+ ions doped zinc alumino bismuth borate glasses. *Spectrochim. Acta A* **2014**, *125*, 53–60. [CrossRef] [PubMed]
122. Nahin, P.G. Infrared Analysis of Clays and Related Minerals. *Clays Clay Miner.* **1952**, *1*, 112–118. [CrossRef]

Disclaimer/Publisher's Note: The statements, opinions and data contained in all publications are solely those of the individual author(s) and contributor(s) and not of MDPI and/or the editor(s). MDPI and/or the editor(s) disclaim responsibility for any injury to people or property resulting from any ideas, methods, instructions or products referred to in the content.